J. Fluid Mech. (1994), *vol.* 263, *pp.* 93–132

Nonlinear dynamics of forced transitional jets: periodic and chaotic attractors

By GEORGE BROZE AND FAZLE HUSSAIN
Department of Mechanical Engineering, University of Houston, Houston, TX 77204-4792, USA

(Received 16 October 1992 and in revised form 27 August 1993)

Conclusive experimental evidence is presented for the existence of a low-dimensional temporal dynamical system in an open flow, namely the near field of an axisymmetric, subsonic free jet. An initially laminar jet (4 cm air jet in the Reynolds number range $1.1 \times 10^4 \leqslant Re_D \leqslant 9.1 \times 10^4$) with a top-hat profile was studied using single-frequency, longitudinal, bulk excitation. Two non-dimensional control parameters – forcing frequency St_D ($\equiv f_{ex} D/U_e$, where f_{ex} is the excitation frequency, D is the jet exit diameter and U_e is the exit velocity) and forcing amplitude a_f ($\equiv u_f'/U_e$, where u_f' is the jet exit r.m.s. longitudinal velocity fluctuation at the excitation frequency) – were varied over the ranges $10^{-4} < a_f < 0.3$ and $0.3 < St_D < 3.0$ in order to construct a phase diagram. Periodic and chaotic states were found over large domains of the parameter space. The periodic attractors correspond to stable pairing (SP) and stable double pairing (SDP) of rolled-up vortices. One chaotic attractor, near SP in the parameter space, results from nearly periodic modulations of pairing (NPMP) of vortices. At large scales (i.e. approximately the size of the attractor) in phase space, NPMP exhibits approximately quasi-periodic behaviour, including modulation sidebands around $\frac{1}{2}f_{ex}$ in u-spectra, large closed loops in its Poincaré sections, correlation dimension $\nu \approx 2$ and largest Lyapunov exponent $\lambda_1 \approx 0$. But investigations at smaller scales (i.e. distances greater than, but of the order of, trajectory separation) in phase space reveal chaos, as shown by $\nu > 2$ and $\lambda_1 > 0$. The other chaotic attractor, near SDP, results from nearly periodic modulations of the first vortex pairing but chaotic modulations of the second pairing and has a broadband spectrum, a dimension $2.5 \leqslant \nu \leqslant 3$ and the largest Lyapunov exponent $0.2 \leqslant \lambda_1 \leqslant 0.7$ bits per orbit (depending on measurement locations in physical and parameter spaces).

A definition that distinguishes between physically and dynamically open flows is proposed and justified by our experimental results. The most important conclusion of this study is that a physically open flow, even one that is apparently dynamically open due to convective instability, can exhibit dynamically closed behaviour as a result of feedback. A conceptual model for transitional jets is proposed based on two-dimensional instabilities, subharmonic resonance and feedback from downstream vortical structures to the nozzle lip. Feedback was quantified and shown to affect the exit fundamental–subharmonic phase difference ϕ – a crucial variable in subharmonic resonance and, hence, vortex pairing. The effect of feedback, the sensitivity of pairings to ϕ, the phase diagram, and the documented periodic and chaotic attractors demonstrate the validity of the proposed conceptual model.

1. Introduction

In recent years, the concept of coherent structures (Kline *et al.* 1967; Crow & Champagne 1971; Brown & Roshko 1974; Lumley 1981; Fiedler 1988) and the

development of dynamical systems theory have led to the hope that low-dimensional, deterministic dynamics may underlie the seemingly random motion in turbulence. Possible connections between dynamical systems and turbulence have been the subject of several review articles (e.g. Lanford 1982; Guckenheimer 1986; Ruelle 1991), which conclude that a dynamical systems treatment of turbulence is possible, in principle. Keefe (1987) suggested that coherent structure eduction methods implicitly assume the existence of an attractor on which conditional averages are performed (not inconsistent with the suggestions of Hussain 1986 and Bridges 1990).

The question as to whether *open* flows – the overwhelming majority of flows in nature and technology – can behave as dynamical systems has been seriously debated in the past decade. The objective of this study is to demonstrate the existence of a dynamical system in an open flow and, thereby, to lay a foundation for future connections between the motions on a strange attractor and vortex formation and interactions in physical space. Circular jets were chosen for several reasons in addition to their simple geometry, construction and wide availability as a laboratory facility: (i) a sequence of axisymmetric (i.e. two-dimensional) instabilities can occur before transition to turbulence, suggesting that low-order nonlinearities may exist; (ii) periodic and non-periodic states have been observed when the flow is periodically forced, suggesting possible transitions to chaos; and (iii) the coherent structures have been well studied previously (e.g. Crow & Champagne 1971; Hussain & Zaman 1980, 1981). In this study, we emphasize the important differences between (*a*) open and closed flows and (*b*) physically and dynamically open flows; moreover, we observe that a physically open flow can behave like a closed flow. The roles of local and global instabilities and *feedback* in closing an open flow are recognized and used to construct a *conceptual model* of jet transition dynamics. Based on this model, a control parameter space is chosen and explored in detail experimentally. The attractors found are investigated using dynamical systems techniques. Our experimental results largely support the conceptual model. Before presenting these results, we briefly review the applications of dynamical systems to fluid flows.

1.1. *Studies of flow systems using dynamical systems techniques*

Confined flows such as Taylor–Couette flow and Rayleigh–Bénard convection have been studied in experiments successfully (e.g. Brandstäter & Swinney 1987; Libchaber & Maurer 1980; Bérge *et al.* 1980) using dynamical systems techniques. Such studies have the advantage that these flows are absolutely unstable or globally unstable, and the boundaries allow only certain discrete sets of eigenfunctions to be selected by the systems at low Reynolds/Rayleigh numbers. Studies of open flows may have neither of these advantages and typically have the disadvantage that the flows are spatially developing; thus, applied to open flows, dynamical systems techniques have produced more limited results. A number of researchers have studied physically open transitional flows using dynamical systems techniques to calculate invariants such as correlation dimension ν, largest Lyapunov exponent λ_1 and Kolmogorov entropy. Sreenivasan (1985) believed that he found a quasi-periodic route to chaos in cylinder wakes for $30 \leqslant Re_D \leqslant 10^4$ (a flow that is absolutely unstable in the near field but convectively unstable in the far field). This result was later contested by Van Atta & Gharib (1987), who found only single-frequency Strouhal vortex shedding in the range $40 \leqslant Re_D \leqslant 160$ unless the cylinder was also vibrating; they concluded that Sreenivasan's ordered and chaotic regimes were due to aeroelastic coupling of the wake with cylinder vibration modes (not considered by Sreenivasan). Yokuda & Ramaprian's (1990) experiments in the cylinder wake for $10^4 \leqslant Re_D \leqslant 10^5$ yielded

positive λ_1 and $\nu \approx 10$–12 (although to estimate such high dimensions with their short time series data is questionable; see Ruelle 1990).

Airfoil wakes were studied experimentally by William-Stuber & Gharib (1990), who found that chaotic behaviour could be achieved via a quasi-periodic route if the flow were forced at two frequencies in addition to the natural shedding frequency. In two-dimensional simulations of airfoil wakes, Rohling *et al.* (1990) found a small window of chaos using angle of attack as a bifurcation parameter, while Vastano & Pulliam (1989) observed period-doubling using a fixed angle and varying speed. Jenkinson & Hussain (1987) found steady and periodic behaviour, but not chaos, in transitional pipe flow using pressure drop as the control parameter. Aronson, Gaponov-Grekhov & Rabinovich (1988) calculated dimension in an excited flat-plate boundary layer, finding $\nu \approx 4$ and ascribing this dimension to the presence of four (ribbon forcing, 'parasitic', ribbon-flow and plate oscillation) frequencies, only one of which was clearly not due to facility vibration or electronic noise. Beyond a certain distance downstream, ν grew linearly with distance; they associated this with the onset of three-dimensionality. In a recirculating jet, they measured $2.5 < \nu < 3$ in an open test section between the jet exit and blower intake. The effects of this odd kind of feedback on the dynamics were alluded to but not discussed; perturbations might have propagated through the return channel or fed back from impingement on the intake. Sreenivasan (1986) found $\nu \approx 6.3$ and $\lambda_1 \approx 0.95$ bits/orbit for an unexcited jet and $\nu \approx 3.2$ for an excited jet (but reported no λ_1); no explanation of the flow physics was offered for either case. For an axisymmetrically excited jet with an exit Poiseuille profile at $Re_D = 543$, Bonetti & Boon (1989) found that dimension increased continuously from $\nu \approx 3$ to $\nu \approx 6$ over the axial range of 18–24 diameters. They found a power-law dependence between spatial coherence and attractor dimension and attributed the low dimension to the persistence of the helical modes. Aubry *et al.* (1988) derived a system of ordinary differential equations for a boundary layer (using proper orthogonal and Fourier modes and Galerkin projection) and analysed invariant subspaces of their dynamical system for regular and chaotic behaviour. Though studying a physically open flow, they used periodic boundary conditions in the streamwise direction, in effect closing the flow dynamics.

1.2. *Organization of the paper*

This paper is organized as follows. In §2, we define open flows, review relevant concepts in stability and feedback, and explain our conceptual model of the jet transition region as a dynamical system. The phase diagram of the jet, measured in the parameter space of forcing frequency St_D and forcing amplitude a_f, is presented and discussed in §3. In §§4 and 5, we investigate two periodic attractors and two chaotic attractors using tools of nonlinear dynamics. Section 6 discusses other states which were recognized but not definitively shown to be low-dimensional or deterministic. In §7, we conclude with some remarks about our results and the applicability of these techniques to open flows in general.

2. Conceptual model of the dynamical system

2.1. *Physically and dynamically open systems*

A definition of open flows The traditional definition of an open flow is one in which fluid does not remain within the domain of interest but crosses its boundaries. Examples include most technological flows such as jets, mixing layers, boundary layers

and pipe flows. The definition that we propose instead is that *an open flow is one in which external perturbations cross the boundaries and dominate the dynamics.* (This definition is not inconsistent with the ideas of Morkovin 1988 and Huerre & Monkewitz 1990.) We refer to the traditional definition as 'physically open' and to our definition as 'dynamically open'.

Since external disturbances may significantly influence, but not necessarily dominate, flow dynamics, being 'open' or 'closed' is clearly a matter of degree. In principle, any combination of 'open' and 'closed' is possible. For example, Biringen & Peltier (1990) simulated three-dimensional Rayleigh–Bénard convection (physically closed) with sinusoidal and random gravity modulations and found changes in both the stability and dynamics of the flow (partially dynamically open). On the other hand, the edgetone generated when (physically open) free shear flows impinge on a wedge can cause phenomena such as single-frequency vortex generation and sound production, the frequency locking being caused by feedback (dynamical closure) from the wedge to the separation point (establishing a global mode; e.g. see Chomaz, Huerre & Redekopp 1988).

The open flow problem Dynamically open flows might not be describable as deterministic dynamical systems because it may not be possible to incorporate the influence of external perturbations in other than a statistical sense. This may seem to contradict the fact that one can formulate Navier–Stokes problems with appropriate initial and boundary conditions. However, in a practical flow, the specified boundary conditions can never be met owing to the presence of external noise. The influence of noise is only a minor problem in dynamically closed flows, because the internal dynamics dominate and the external noise serves to randomize the dynamics only at the smallest scales in phase space (e.g. to spread trajectories slightly on a limit cycle). In dynamically open flows, however, noise dominates the evolution of the system (e.g. see Deissler 1989), which can hence be described as 'noise-driven'. Therefore, *the 'open flow problem' is the inability to predict the dynamics of open flows.* This is obviously a very serious constraint on our ability to predict and control turbulence.

Whether a flow is open or closed depends strongly on the instability type (i.e. absolute or convective), a major component of the dynamical system. This is discussed more fully below.

2.2. *Absolute and convective instabilities and global modes*

This discussion of instability is limited to spatially developing, physically open flows. Local flow instabilities (i.e. due to the velocity profile) can be classified as either absolute or convective. In an absolutely unstable (AU) flow, disturbances spread upstream and downstream and influence the entire flow, and, moreover, are continually felt at their *points of origin.* In a convectively unstable (CU) flow, disturbances are advected away from the source; i.e. all unstable wavenumbers have non-zero group velocity. Free shear flows may fall into either category, but are generally CU (see Huerre & Monkewitz 1990).

These spatially local stability concepts do not preclude the existence of global modes (resulting from an instability of the entire flow domain of interest). (However, even flows with *global* modes may depend on *local* instabilities, e.g. Kelvin–Helmholtz instability in a shear layer tone.) By global modes, we mean oscillations that are self-sustained (via feedback, if locally CU) and occupy an extended spatial domain, i.e. $\lambda/L \ll 1$ where λ is disturbance wavelength and L is domain size. (As an example, for a jet disturbance travelling at half the jet speed, $\lambda/D = (2\,St_D)^{-1}$; if $St_D = 1$ and $L = 5\,D$, $\lambda/L = 0.1$.) Huerre & Monkewitz discuss global instabilities extensively with

an emphasis on flows with regions of absolute instabilities (e.g. near wakes and heated jets) which drive downstream convective instabilities; they describe the preferred mode of cold jets as a slightly damped global mode maintained by low-level forcing. It is not clear that such forcing is required, since the preferred mode has been (and, indeed, is typically) observed without controlled forcing. In this paper, we emphasize global modes arising from *feedback* (in CU flows with no known AU regions), specifically from the open domain (rather than from impingement as discussed by Chomaz *et al.* 1988).

Spatially developing free shear flows have points of receptivity, such as a jet nozzle lip or the trailing edge of a mixing-layer splitter plate, which act as the origin from which disturbances grow. The fact that the disturbances advect away in a CU flow leaves this origin *open* to respond to new disturbances which may originate external to the flow domain (i.e. sources not due to flow, such as facility noise and ambient acoustic perturbations); a growing disturbance does not remain spatially fixed to dominate dynamics at its inception point as it does in an AU flow.

The differences between absolute and convective instabilities have important implications for flow dynamics, perhaps first recognized by Deissler (1985) and Huerre & Monkewitz (1985). In the absence of external disturbances (except some initial perturbation to trigger the instabilities), an AU flow will behave asymptotically according to its own internal dynamics, reaching some saturated nonlinear state, e.g. convection rolls in Rayleigh–Bénard convection or vortices shed from a cylinder in cross-flow at low Re_D. In contrast, a pure CU flow has asymptotically only a trivial steady state, since all disturbances will eventually advect out of any finite domain. (By 'pure' CU flow, we mean one in which feedback, and hence global modes, are absent.) Pure CU flows can have non-trivial dynamics only if there is continuous input of external disturbances; phenomena seen at any point in space are upstream (usually free-stream) perturbations transformed into waves, vortices, etc., through what is now called 'receptivity'. Although these phenomena are typical events in the system, their occurrence cannot be predicted in time because the perturbations that trigger them are random. On the other hand, *periodic* forcing can be used to regularize these phenomena and could easily be incorporated into a mathematical model analytically as a time-dependent (but deterministic) inflow boundary condition. This is not true of stochastic forcing, unless its time history (and not only its statistics) could be precisely specified. Regardless of the nature of the external perturbation, however, pure CU flows clearly are dynamically open.

One may argue that global solutions must occur, even in CU flows, owing to the elliptic nature of pressure in Navier–Stokes flows, but this is not necessarily true. While fluctuations within the domain must be felt at the boundaries due to ellipticity, these fluctuations must compete with external perturbations (i.e. noise) at the point of receptivity. Noise may dominate effects from elsewhere in the domain (again, a result of the flow being open).

Dynamical systems models of CU flows (e.g. Aubry *et al.* 1988, boundary layers; Glauser, Zheng & Doering 1991, jets) have been developed and analysed, showing such results (from Aubry *et al.*) as periodic behaviour, heteroclinic chaos and sensitivity to external perturbations. However, these models were developed using periodic boundary conditions in the streamwise direction, thus enforcing an artificial dynamical closure: all perturbations advecting out through the downstream boundary re-enter the domain through the inflow boundary. This is mathematically convenient but may not model the actual dynamics of these convectively unstable, spatially developing flows. In the actual flows, feedback may close the dynamics, but (i) the presence of feedback was not

established in these studies and (ii) its effects are unlikely to be correctly modelled by periodic boundary conditions.

2.3. *Feedback and dynamical closure*

The way in which locally CU flows can be dynamically closed is by feedback, either from solid boundaries or from flow events within the domain. Feedback has two important consequences. First, the system can govern its own dynamics by driving itself with perturbations from downstream, even though the flow is locally CU. Second (as a result), global modes can occur, implying that the motion is correlated in an entire region. Thus, while the spatial structure is important, the dynamics of the global mode may be describable by measurements at a limited number of positions. *Dynamical closure implies that the flow may act as a temporal, perhaps low-dimensional, dynamical system.* Closure is obviously crucial if dynamical systems approaches are to describe and model CU flows.

Feedback can have a variety of sources. Huerre & Monkewitz (1990) point out that global instability can arise from upstream-propagating vorticity waves and from irrotational pressure feedback; whereas the former case is not likely in CU flows, the latter is. The pressure feedback is governed in the incompressible, inviscid limit by a Poisson equation $\nabla^2 p = -\rho\,\partial_i\,\partial_j(u_j u_i)$. This equation can be transformed into $\nabla^2 p = \rho(\frac{1}{2}\omega^2 - \boldsymbol{s}:\boldsymbol{s})$, linking pressure directly to vorticity and strain rate tensor $\boldsymbol{s}$; changes in vorticity must be accompanied by changes in the pressure field – the basis of vortex sound theory. They further state that the potentially most powerful sources are found when the flow encounters boundaries (of or within the flow domain), although '"volume sources" such as "vortex pairing"... may also be significant'. The role of solid boundaries is seen in many examples, such as edgetones, whistler nozzles, impinging jets and flow over open cavities. Even artificial boundaries such as those necessarily imposed in numerical simulations that use inflow–outflow boundary conditions can unintentionally result in global modes (Buell & Huerre 1988). If downstream boundaries and flow obstacles are not significant, volume sources may be important, however. Dimotakis & Brown (1976) measured very long autocorrelation times in a two-stream mixing layer and hypothesized that there was coupling (via vortex-induced motion) between the trailing edge of the splitter plate and structures exiting the test section, which kept the newly forming structures in phase with the exiting ones. Laufer & Monkewitz (1980) used a feedback model of vortex pairing to explain the pairing locations found experimentally by Kibens (1980) in an excited jet. Based on phase locking, the subharmonic period must equal the advection time from the lip to the pairing location plus the acoustic feedback time with feedback being generated by vortex pairing ('volume source').

2.4. *Evidence of feedback*

While Dimotakis & Brown (1976) and Buell & Huerre (1988) observed the *effects* of feedback in mixing layers, Grinstein, Oran & Boris (1990) provided more direct evidence by simulating the initial rollups of a compressible plane mixing layer in a large domain. They stopped the simulation well before the startup vortex reached the outflow so that only feedback from events within the flow domain, and not from numerical outflow boundary conditions, would be felt. They found that pressure waves, generated at rollup, propagate upstream to trigger subsequent instability waves, and they suggested that the difference between propagation speeds in the two streams creates a phase difference across the layer which provides a transverse velocity perturbation when the pressure wave reaches the inflow. This provides a direct link

between feedback and unsteady vorticity in the shear layer. Note that this feedback is due to rollup rather than pairing.

Numerical results in our laboratory also point to the role of in-domain feedback. Simulations of an incompressible, two-dimensional, viscous mixing layer with a splitter plate (Virk 1989) showed $St_{\theta e} \approx 0.012$, implying a role for feedback similar to that of Hussain *et al.* (1986). Virk used a finite-element scheme with outflow boundary conditions $\partial\omega/\partial n = 0$, but a convective outflow condition ($\partial\omega/\partial t + c\,\partial\omega/\partial x = 0$) also showed similar results. Two different domain sizes were used with no apparent differences in $St_{\theta e}$. Vortex filament simulations of interacting vortex rings by Bridges (1990) show that the peak amplitude of the sound generated occurs when the rings are coplanar, as occurs only at a particular phase of vortex pairing. The generated sound is a mechanism by which perturbations could be transmitted to the lip.

Experimental evidence also supports the presence of feedback. Hussain *et al.* (1986; based on measurements by Hussain & Zaman 1978) found that when the circulation (estimated from the saturation amplitude) is divided by the distance from the splitter plate to the saturation location (approximately the relative amplitude of the Biot–Savart vortex-induced motion), its maximum value occurs near $St_{\theta e}$ ($\equiv f_{ex}\theta_e/U_e$, θ_e being the momentum thickness at the lip) ≈ 0.012, which is the observed 'natural' frequency in many mixing-layer experiments but *not* for the fastest growing mode ($St_{\theta e} \approx 0.017$). This suggests that the system is dominated by the frequency that provides the most self-excitation rather than the one with the largest growth rate. From the present experiments, figure 1(*a*) shows the jet-exit centreline fundamental–subharmonic phase difference ϕ_{out} as a function of forcing-signal phase difference ϕ_{in} in cases where periodic pairing (and double pairing) does ($St_D = 1.17$) or does not ($St_D = 3.33$) occur. (Two-frequency forcing, f and $\frac{1}{2}f$, was employed with controlled ϕ_{in}; phase difference calculations are described in the Appendix, §A.2.) When SP and SDP (and hence strong, periodic feedback) occur, the superposition of forcing and feedback should create a nonlinear relationship between $\phi_{in} - \phi_{out}$ (since feedback is stronger at those phase differences for which pairing is closer to the jet exit, which is the case for SP and SDP). When stable pairings do not occur, pairing feedback should be weaker and the $\phi_{in} - \phi_{out}$ relationship should be linear. This is clearly the case in figure 1(*a*). Second, this feedback should be evident in exit velocity fluctuations. Exit-centreline spectra using single-frequency excitation ($f_{ex} = 264$ Hz) are shown for the 'fundamental only' state (i.e. excited near the preferred mode frequency and exhibiting no pairings; figure 1*b*) and stable double pairing (figure 1*c*). In the first case, there is clearly no subharmonic content in the exit spectrum, while in the second case sharp peaks are seen at $\frac{1}{2}f_{ex}$ and $\frac{1}{4}f_{ex}$ (132 and 66 Hz respectively) reflecting periodic feedback.

2.5. *Subharmonic resonance*

Primary instability The primary instability in free shear layers and jets is the (two-dimensional) Kelvin–Helmholtz instability. For linear instability theory, see Michalke (1965) for spatially developing mixing layers and Michalke (1971) for circular jets with different ratios of jet radius to momentum thickness. The physical result of a saturating Kelvin–Helmholtz wave is the 'rollup' of the wave into a vortex. These vortices and those formed by their interactions in transitional flows are equivalent to coherent structures in turbulent flows.

Subsequent to the formation of Kelvin–Helmholtz vortices, there are two well-known subharmonic instabilities in free shear flows: 'pairing' and 'tearing' or 'shredding' (e.g. see Kelly 1967; Patnaik, Sherman & Corcos 1976; Pierrehumbert & Widnall 1981; Corcos & Sherman 1984; Monkewitz 1988). Pairing is the interaction of

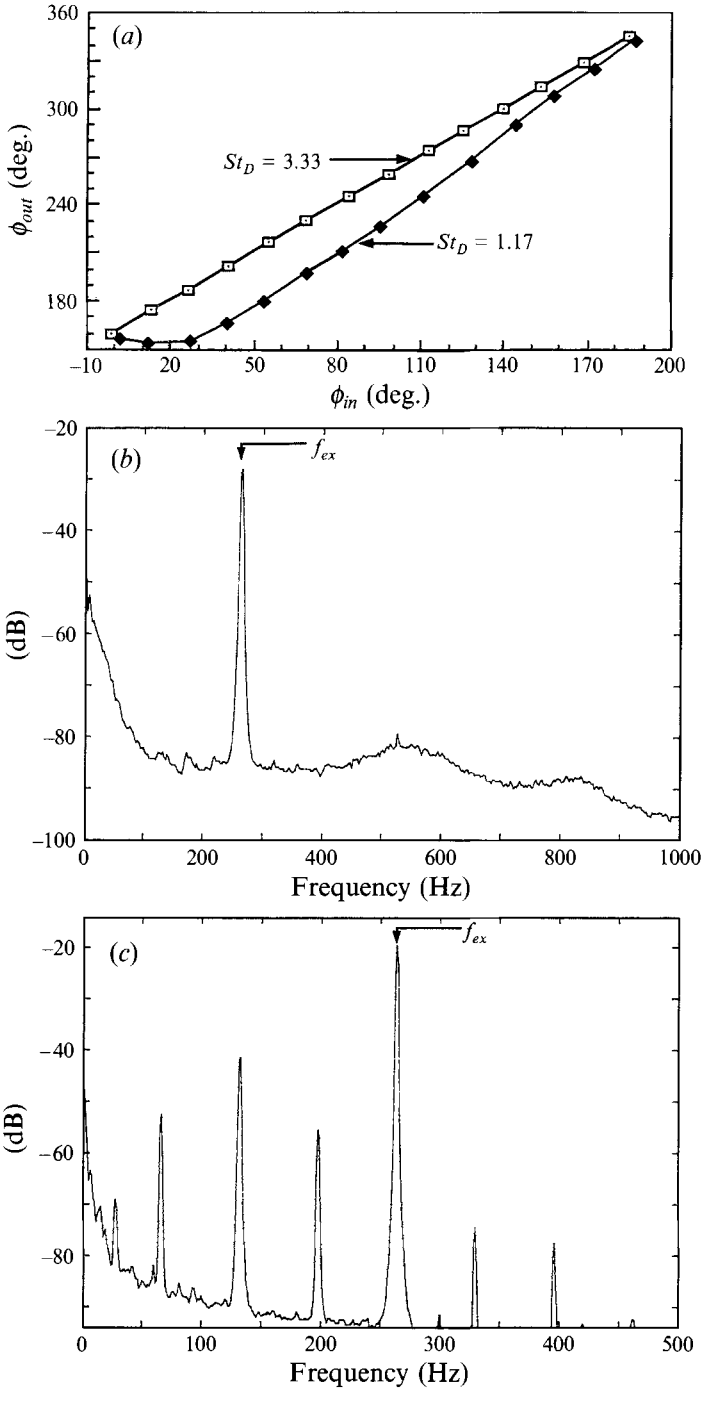

FIGURE 1. (*a*) Influence of forcing phase difference ϕ_{in} between fundamental and subharmonic on jet exit phase difference ϕ_{out} at two fundamental St_D values. (*b*) Jet exit power spectrum of u for fundamental only at $St_D \approx 0.40$, $a_f \approx 1.00\%$, $Re_D \approx 6.9 \times 10^4$, $x/D = 0$. (*c*) Jet exit power spectrum of u for stable double pairing at $St_D \approx 1.19$, $a_f \approx 2.4\%$, $Re_D \approx 2.3 \times 10^4$, $x/D = 0$.

two vortices in which they revolve around each other, eventually merging through the action of viscosity to form a single core. Tearing occurs when a vortex is caught in the opposing induced fields of two stronger (nearly equal) vortices which shear it into two segments, each merging with the nearby vortex. Both interactions need only be two-dimensional. Since pairing provides feedback to close the jet dynamics, some relevant results are summarized below.

Subharmonic instability was studied using nonlinear temporal theory for a periodic base flow by Kelly (1967), who found that there are four main requirements for subharmonic (s) resonance: (i) a 2:1 wavenumber ratio, (ii) a threshold amplitude ($\approx 12\%$ of the velocity difference) of the fundamental (f) wave in order for the s growth rate to exceed that of the most unstable disturbance of the mean flow, (iii) equal phase speeds and (iv) f near neutral (i.e. near saturation). While the phase speed requirement is met in the temporal theory automatically (all phase speeds are equal), phase speeds and wavenumber ratio cannot both meet the resonance condition in the linear spatial theory (Monkewitz 1988). Monkewitz found a critical fundamental amplitude for the nonlinear, spatially developing case, about which the initial gap between f and s phase speeds was closed asymptotically (by slowing or accelerating the s-wave via nonlinear interaction), and resonance occurred. He further found that the initial resonant growth rate of s depends on the cosine of the phase angle ϕ between the two waves. During the time interval in which the phase speeds become matched, phase continually shifts, so that even when s is initially damped, ϕ will shift to an amplified value except for a critical angle $\phi_c = 0.064\pi$. The length of this interval, hence the location of the onset of resonance, varies with ϕ. Thus, s-amplitude measured at a location between the f and s saturation locations should be periodic in ϕ with a cusp-like attenuation at ϕ_c.

Mixing-layer experiments on subharmonic resonance were performed by Husain & Hussain (1986, 1989) using two-frequency (fundamental f and subharmonic $\frac{1}{2}f$) excitation with controlled amplitudes and ϕ_{in} (the phase difference between f and $\frac{1}{2}f$ at the lip). They documented a strong effect of ϕ_{in} on the s growth rate and a cusp-like amplitude response; they also studied the effects of detuning (the interaction of waves at two frequencies f and $\frac{1}{2}f \pm \Delta f$), which provides a periodic amplitude modulation of s. In addition to the ϕ_{in} dependence, jet experiments in our laboratory by T. Liu (private communication, 1991) using two-frequency ($f, \frac{1}{2}f$) excitation showed significant effects of forcing amplitudes, including hysteresis in the s growth rate as a function of ϕ.

An analysis of f–s interactions in turbulent, round jets was done by Mankbadi (1985) using energy methods. He derived a set of nonlinear ordinary differential equations for component evolutions. He confirmed the dependence of the s growth rate on the fundamental frequency f and found that the number of amplified subharmonics (i.e. $\frac{1}{2}f$, $\frac{1}{4}f, \ldots$) depends on St_D; e.g. three pairings will occur at $St_D = 2.4$, producing subharmonics at $St_D = 1.2$, 0.6 and 0.3.

2.6. *Jet breakdown*

At some stage of jet transition, three-dimensional instabilities will become important, resulting in the formation of streamwise vortical structures (so-called 'ribs') between spanwise vortices. These distort the rings and cause local vortex interactions which lead to the breakdown of the two-dimensional structures. Such interactions may not provide organized feedback at sufficient amplitudes to cause low-dimensional deterministic dynamics. (Although induced perturbations at the jet exit from three-dimensional compact events can be viewed as nearly two-dimensional when the events are far downstream, the induced motions would be weaker.) Since our model for dynamical closure requires strong feedback (i.e. greater than the noise level), it is not

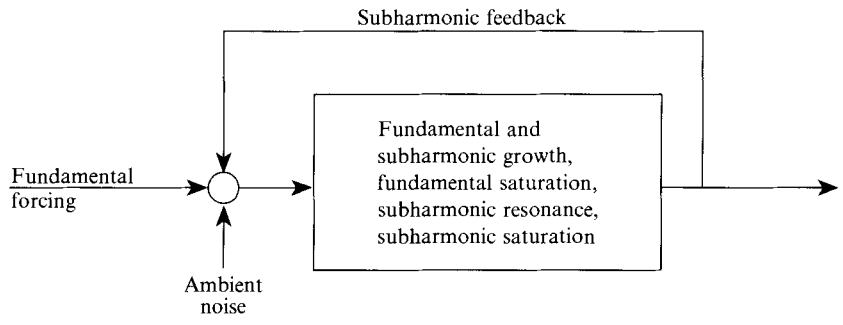

FIGURE 2. Conceptual dynamical system of transitional jets.

likely that our dynamical system would persist beyond the near-exit, two-dimensional region.

2.7. *Conceptual model for transitional jet dynamics*

The theoretical, numerical and experimental evidence of subharmonic resonance and feedback have led us to hypothesize the system shown in figure 2. From initial perturbations, the fundamental (f) and subharmonic (s) grow independently at exponential rates determined by their frequencies, according to linear theory. After f reaches a critical amplitude, f and s resonate, modifying the growth rate of s. As s saturates, its feedback amplitude at the lip reaches a maximum, initiating the next s wave. For the second subharmonic, a second stage of resonance and feedback would be added.

Dynamical variables The key dynamical variables are the fundamental amplitude a_f, subharmonic amplitude a_s and the f–s phase difference ϕ. In the case of two successive subharmonic interactions, the quarterharmonic (q) amplitude and the s–q phase difference would also be important. In our experiments, we control St_D and initial fundamental amplitude a_f at the jet exit, allowing a_s and ϕ to evolve naturally. Since it seems that the crucial nonlinearity comes from subharmonic resonance in which the growth of s depends on $\cos\phi$, it is important to understand how feedback controls ϕ. If the time τ_{fb} from initiation of s until its feedback reaches the lip is equal to the s period τ_s, then ϕ will be the same as before, since f is periodically forced with a period $\tau_f = \frac{1}{2}\tau_s$. Since ϕ is the same, the resonant s growth rate should be the same, as should the overall spatial evolution of s. This phase locking results in periodic flow, i.e. stable pairing. However, if $\tau_{fb} \neq \tau_s$, ϕ will be different from one period to the next, resulting in a growth rate, saturation location and subsequent feedback time different from the previous cycle. Therefore, ϕ will wander, perhaps periodically or chaotically, as will the s-amplitude measured at a location downstream of the lip.

The previous discussion explains the role of ϕ only. In addition, the exit s-amplitude a_{se} (due to feedback) also affects τ_{fb}; however, the saturation location (and hence time to saturation) varies only as $-\log a_{se}$, so that this effect may not be as pronounced. If phase-locked, then it is likely that the feedback amplitude is also the same from one pairing to the next, thereby leading to the same a_{se} each time. However, when not phase-locked, a_{se} will also vary from period to period, increasing the number of degrees of freedom. In the light of this, it is somewhat remarkable that SP and SDP exist with only fundamental excitation.

Forcing The downstream events in transition are largely controlled by perturbations at the exit. Since the primary instability has a (continuous) broadband receptivity spectrum, forcing plays a key role in controlling the dynamical system. By periodically exciting at a particular unstable frequency, preference is given to that mode as well as

modes that resonate with it, and the degrees of freedom are reduced in effect to a small number. Furthermore, by choosing a value of St_D, the frequencies of f and s are fixed, dictating their (linear theory) growth rates and the saturation amplitude of f. Given these, the forcing amplitude a_f controls the saturation location of f (Freymuth 1966) and thus influences the saturation locations of the subharmonics. Thus a_f and St_D directly or indirectly control many features of the downstream evolution.

Noise The effect of noise in this system is to compete with feedback and to disrupt the global mode dynamics. When a_f is high, noise is unlikely to affect f but may affect s, whose amplitude at the jet exit is much lower (see figure 1*b*) since its only source is feedback. At lower a_f, noise may interfere with the evolution of both f and s. In either case, noise can alter amplitudes and phase difference when superposed with forcing or feedback, or even excite a different unstable frequency, changing the dynamics of the system from self-driven to noise-driven.

Summary The elements of linear stability, subharmonic resonance and feedback can be combined to explain how global modes can occur which permit the jet transition region to behave as a dynamical system. Convective instabilities render the system open, but feedback closes it. Feedback is shown to occur in numerical and experimental flows. The key dynamical variables are the amplitudes of the fundamental and subharmonic(s) and their phase difference(s). The role of forcing is to control the primary instability and hence to limit the number of degrees of freedom of the system, while noise can disrupt the dynamics of the global modes, leading to an open system.

Having presented the essential elements of the conceptual dynamical system, the experimental results to verify it are presented: (i) the phase diagram (§3), (ii) periodic attractors (§4), (iii) chaotic attractors (§5), and (iv) other observed states (§6).

3. Phase diagram

3.1. *Choice of parameters*

Since the Kelvin–Helmholtz instability is broadband, there are many possible choices for the control parameters (e.g. the frequencies and amplitudes of any number of pure tones, phase angles between harmonically related tones). In this work, however, we are interested in the dynamics of modes at *undriven* frequencies, specifically the subharmonics of the (fundamental) vortex rollup frequency; hence we used a single-frequency excitation.

The control parameters chosen are the non-dimensional forcing frequency St_D and amplitude a_f. These two parameters are natural choices, especially if one thinks of the jet as a driven nonlinear oscillator, where frequency and amplitude are the standard control parameters.

There is some question as to whether the appropriate lengthscale to non-dimensionalize frequency should be jet diameter D or exit momentum thickness θ_e, since modes scaling on both of these occur in jets (Michalke 1971; Crow & Champagne 1971; Zaman & Hussain 1980). Since the phenomena being studied involve the entire jet transition region, one would expect D to be the relevant lengthscale. For example, stable pairing has been seen in a number of jets at $St_D \approx 0.85$ regardless of $St_{\theta e}$ (e.g. Zaman & Hussain 1980; Bridges 1990). The flow seems to be relatively independent of Re_D ($\equiv U_e D/\nu$), as long as an initially laminar, top-hat profile is maintained.

Since environmental and facility noise is present in any experiment and is crucial in convectively unstable flows, its amplitude and frequency band should also be considered as parameters. In the experiments presented in this paper, every attempt has

been made to minimize noise, using the low-noise jet facility in our anechoic chamber described in the Appendix, §A.1. The effects of noise on the flow dynamics have been studied and will be presented in a later paper.

3.2. *Paths in the parameter space*

Any path to a given point in the parameter space will lead to the same state when multiple solutions are absent. Typically, the path we used was to fix St_D and vary a_f, monotonically increasing it in small increments (5–15% of the previous level), then monotonically decreasing to check for hysteresis (i.e. multiple solutions). No investigation was made of other paths.

St_D can be changed by varying f_{ex}, U and D in any combination. Because of the discrete resonances of the settling chamber and the desire to explore moderate to high excitation amplitudes ($a_f \leqslant 20\%$), f_{ex} and D were fixed ($f_{ex} = 264$ Hz and $D = 4.0$ cm) and U_e was varied to change St_D. Independently, u_f' was varied to change a_f.

Having made parameter changes, settling times of only a few seconds were typically required. Near transition points, however, as much as several minutes were allowed. Near hysteresis jumps, up to 20 minutes (several hundred thousand periods of f_{ex}) were allowed.

3.3. *Discussion of the phase diagram*

Figure 3(*a*) shows all measurement locations and states found in the parameter space over the ranges ($0.3 \leqslant St_D \leqslant 2.9$, $0.001 \leqslant a_f \leqslant 0.3$). (Nothing of interest was found for $10^{-4} \leqslant a_f \leqslant 10^{-3}$; this region is not shown.) The states shown are found as a_f is increased; slight shifts occur due to hysteresis as a_f is decreased near ($St_D \approx 1.2$, $a_f \approx 1\%$). Nine states are denoted: (i) fundamental only (FO), (ii) stable pairing (SP), (iii) nearly periodic modulations of pairing (NPMP), (iv) stable pairing with modulated quarter-harmonic (SPMQ), (v) stable double pairing (SDP), (vi) quarter-harmonic chaos (QCA), (vii) modulated subharmonic (MOD S), (viii) modulated subharmonic and quarter-harmonic (MOD SQ), and (ix) intermittency (INT). None of the periodic or chaotic states were found for $St_D \geqslant 1.7$ or $a_f \leqslant 0.001$, and these regions were excluded from detailed investigation. Regions where each state exists are pattern-coded and displayed in figure 3(*b*) for ($0.5 \leqslant St_D \leqslant 1.5$, $0.001 \leqslant a_f \leqslant 0.3$); its dominant features are the regions where the periodic attractors are found, labelled SP and SDP. Chaos (QCA and NPMP) is found in smaller regions (labelled 'SP, NPMP, AM', and quarter-harmonic chaotic attractor or QCA). SP and SDP are separated by SPMQ, a state characterized by stable pairing but weaker, modulated quarter-harmonic oscillations (denoting non-stationary second pairing). Other modulated states (MOD S and MOD SQ) are not distinctive and are therefore combined in figure 3(*b*) under the title aperiodic modulations (AM). In this paper, 'modulations' refers to both amplitude and frequency modulations unless otherwise noted. For FO, dominant oscillations occurred only at f_{ex}.

In addition to these measurements, the streamwise evolutions of the fundamental and subharmonics were measured and are presented in the Appendix, §A.4.

High-amplitude excitation was not explored for St_D less than unity owing to constraints of the excitation system. At larger St_D, however, it is seen that SDP does *not* persist for a_f much above 10%, but gives way to modulations, intermittency and chaos with some hysteresis, as it does at lower a_f. These phenomena are interesting (since they show that phase can become unlocked at high as well as low a_f), but, owing to finite increments of the forcing controls at such high amplitudes, it is difficult to achieve the fine resolution in a_f necessary to explore this in more detail. However, these aperiodic states seem to be qualitatively the same as those seen at lower a_f.

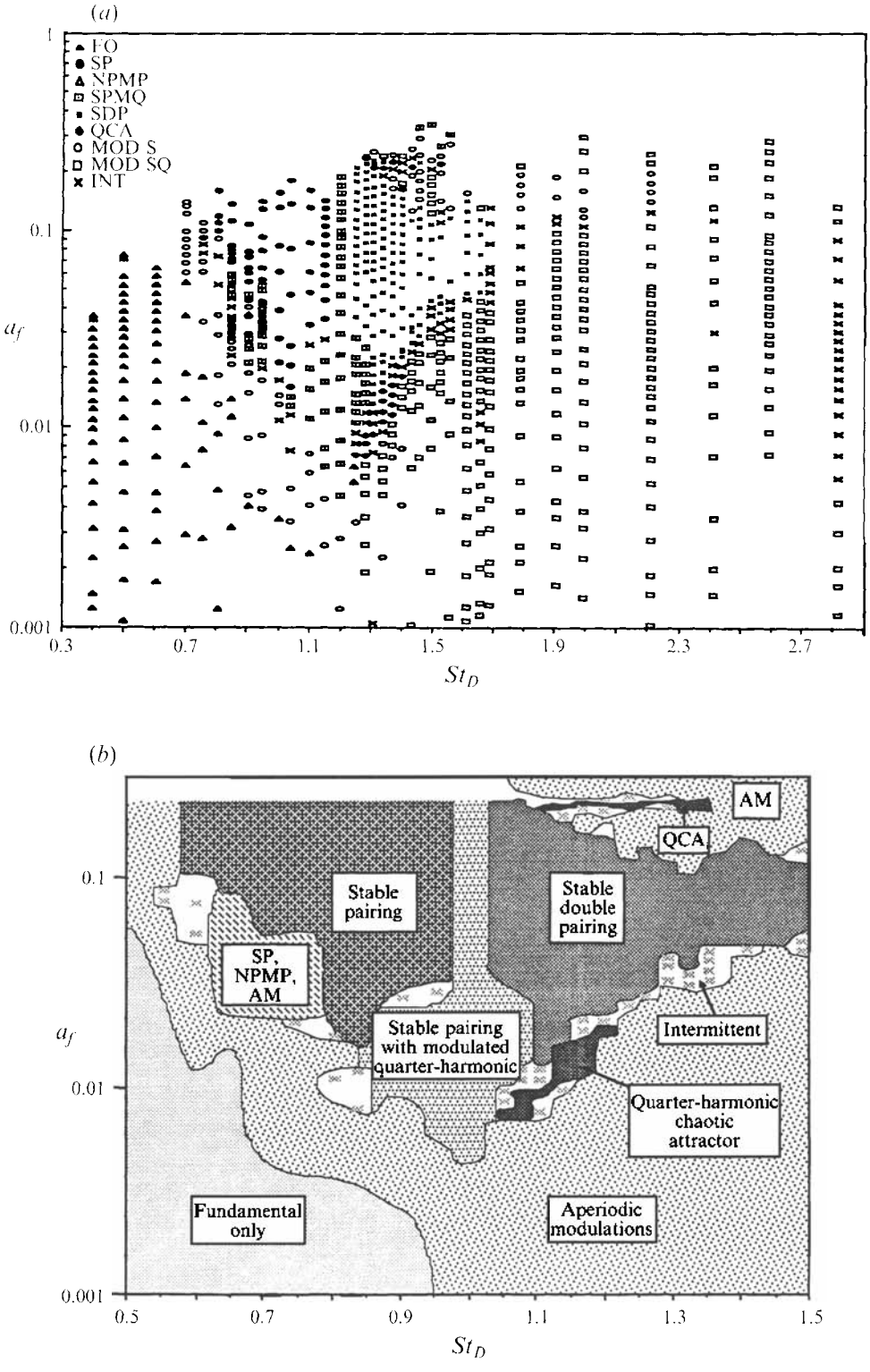

FIGURE 3. (*a*) Sample locations and states observed in the (St_D, a_f) parameter space. (*b*) Phase diagram of the transitional jet in the (St_D, a_f) parameter space, inferred from (*a*).

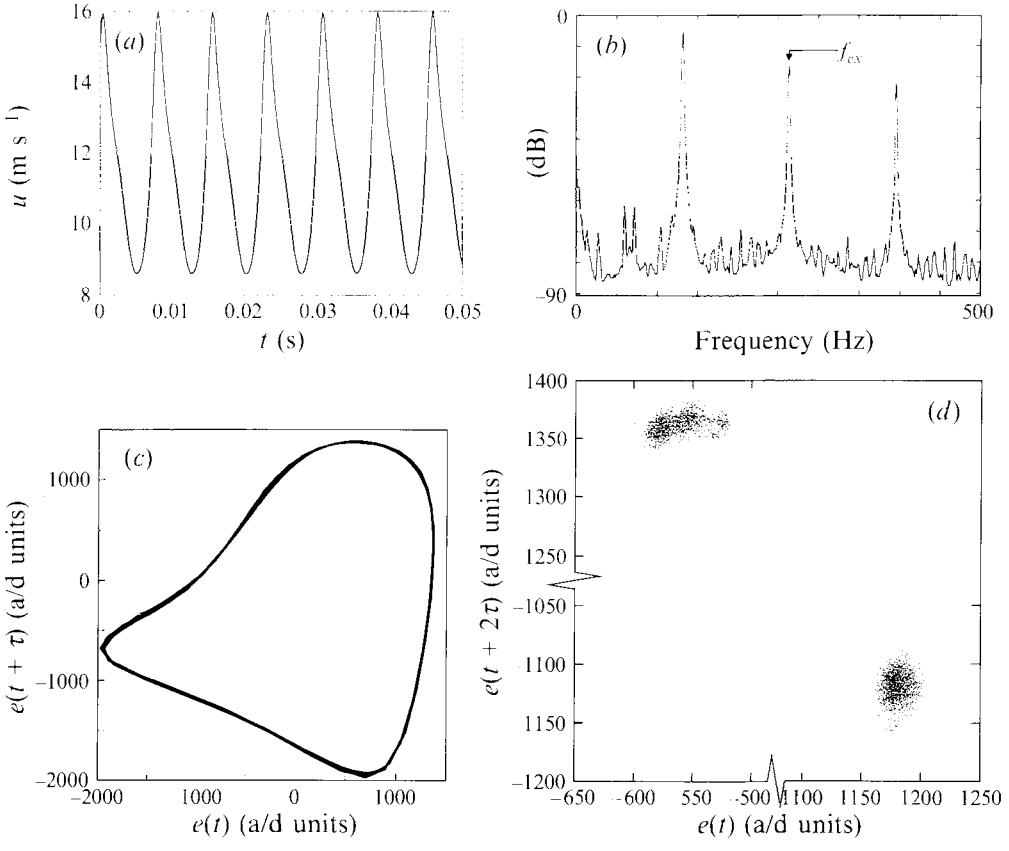

FIGURE 4(*a–d*). For caption see facing page.

3.4. *Results in another facility*

The existence of periodic and chaotic attractors in forced jets is apparently robust. A limited phase diagram was measured in a different axisymmetric jet in our open laboratory (rather than the anechoic chamber) and is presented in Broze & Hussain (1991); this is in substantial agreement with figure 3. In both experiments, SP and SDP were found. While NPMP and QCA were not definitively observed in that work, chaos was found near SP and SDP in the open-lab experiments, as was an intermittency transition to chaos.

In §§4 and 5, the reconstructed attractors are analysed for periodicity or chaos using a variety of techniques: spectra, phase portraits, Poincaré sections and estimation of correlation dimension ν and largest Lyapunov exponent λ_1. Details of these procedures are given in the Appendix, §A.3.

4. Periodic attractors

4.1. *Stable pairing*

Figure 4(*a*) shows a characteristic signal for stable pairing. The signal is periodic with dominant period $\tau = 2/f_{ex} = 0.00758$ s, and there is very little variation of the waveform amplitude or shape. Correspondingly, the spectrum (figure 4*b*) is dominated by sharp peaks at the subharmonic $\frac{1}{2}f_{ex} = 132$ Hz and its harmonics. The highest peak is roughly 60–70 dB above the background, indicating a low-noise signal. There are

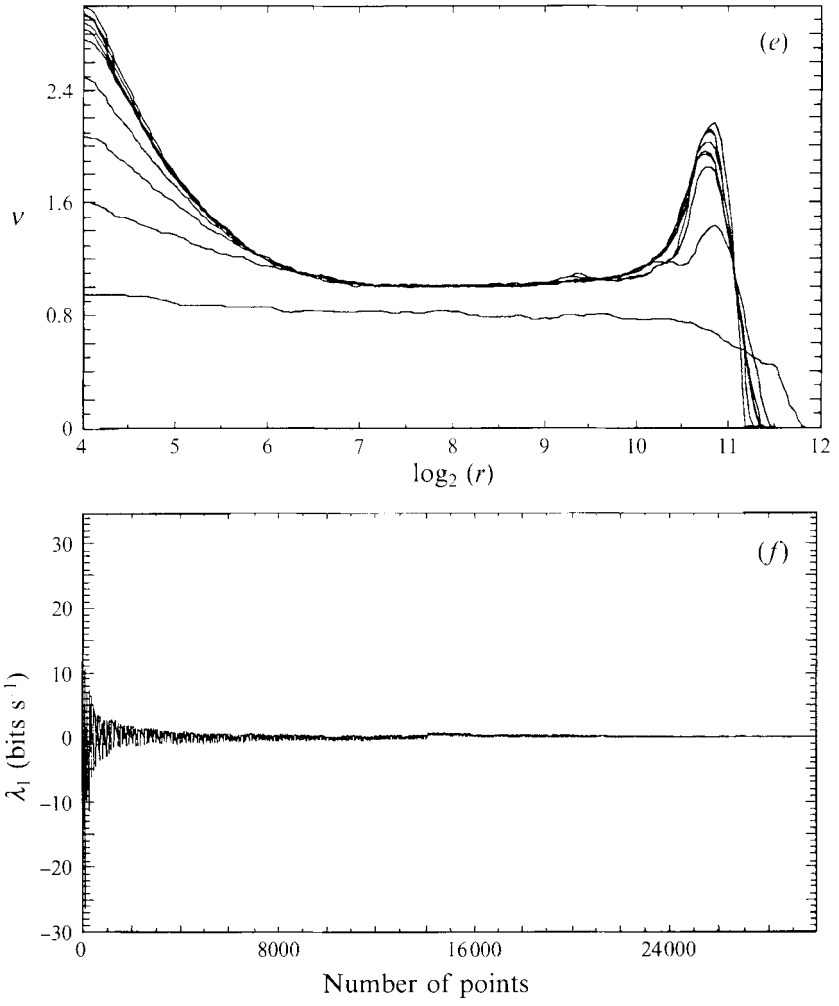

FIGURE 4. Characteristics of stable pairing at $St_D = 0.85$, $a_f = 2.89\%$, $Re_D = 3.3 \times 10^4$, $x/D = 2.0$: (*a*) $u(t)$ signal; (*b*) power spectrum of u; (*c*) phase portrait; (*d*) Poincaré section; (*e*) correlation dimension; (*f*) largest Lyapunov exponent.

weak sidebands of these peaks and a small, low-frequency peak, suggesting a slight amplitude modulation. In addition, there is a pair of low-amplitude peaks centred on the quarter-harmonic ($\frac{1}{4}f_{ex} = 66$ Hz), indicating, presumably, infrequent as well as incomplete second pairings.

A phase portrait (figure 4*c*) was reconstructed using time-delay embedding of the digitized signal. As expected, this reveals a closed loop. Poincaré sections were constructed on planes through the origin inclined at 135° and 315° and are superposed in figure 4(*d*) in the $(e(t), e(t+2\tau))$-plane. The clusters of positive and negative crossings have standard deviations of 20.3 and 14.7 units respectively, and their centroids are separated by 3034 units. The tight cluster distribution relative to their separation distance is evidence of the low noise level. Note that parts of the axes are excluded in figure 4(*d*) in order to reveal the details of the clusters, showing no recognizable structure.

The correlation dimension (figure 4*e*) was determined to be $\nu \approx 1.04$ with scaling limits $x_{min} = 6.25$ and $x_{max} = 10.23$ ($x \equiv \log_2 r$, where r is the distance in phase space).

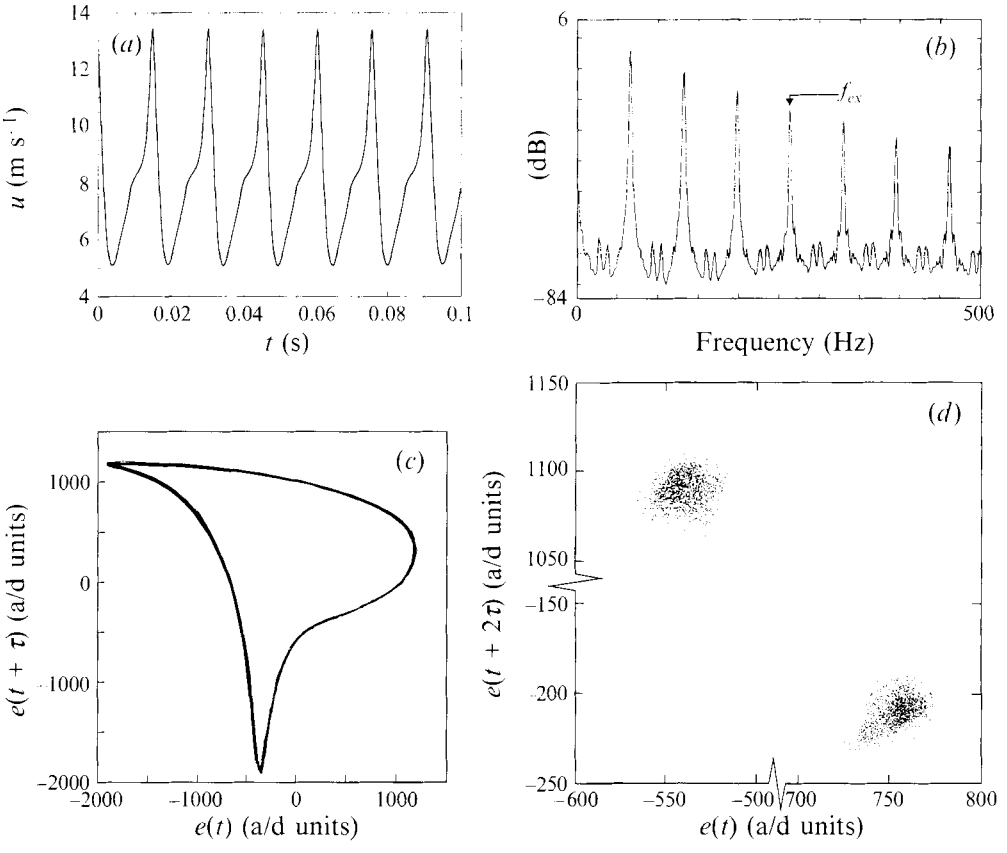

FIGURE 5(*a–d*). For caption see facing page.

These limits correspond to a scaling factor of $2^{3.98} \approx 16$, which is fairly large for typical experimental data. (The scaling factor is the ratio of the largest to the smallest distances in phase space at which scaling is seen.) This dimension value and large scaling factor is consistent with a low-noise limit cycle. Figure 4(*f*) shows the estimate of λ_1 converging to approximately $\lambda_1 \approx 0.35$ b.p.s. (bits per second) or 0.002 b.p.o. (bits per orbit). Based on our experience with the Wolf algorithm, values of $0 \leqslant \lambda_1 \leqslant 0.01$–$0.02$ b.p.o. are not large enough to be considered definitely positive and probably represent a zero value of λ_1 to within the margin of error.

4.2. *Stable double pairing*

The other periodic attractor found in this parameter space is SDP. From the phase-locked measurements of SDP at $St_D = 1.17$ (Bridges & Hussain 1992), it seems that full merger of four vortices does not take place; in their measurements, the leading paired vortex interacts with two trailing vortices, and only one of the trailing pair merges with the leading vortex. It is unknown whether a complete merger would occur elsewhere in the parameter space. Nonetheless, this state is characterized by a strong quarter-harmonic. Figure 5(*a*) shows a sample time trace of SDP; the trace is periodic with period $\tau = 4/f_{ex} = 0.0152$ s and shows little variation of the waveform or the amplitude. The spectrum (figure 5*b*) is dominated by sharp peaks at $\frac{1}{4}f_{ex} = 66$ Hz and its harmonics, with the highest peak rising 70 dB above the background. There are low-amplitude sidebands around $\frac{1}{8}f_{ex}$ (and odd harmonics), analogous to those found near

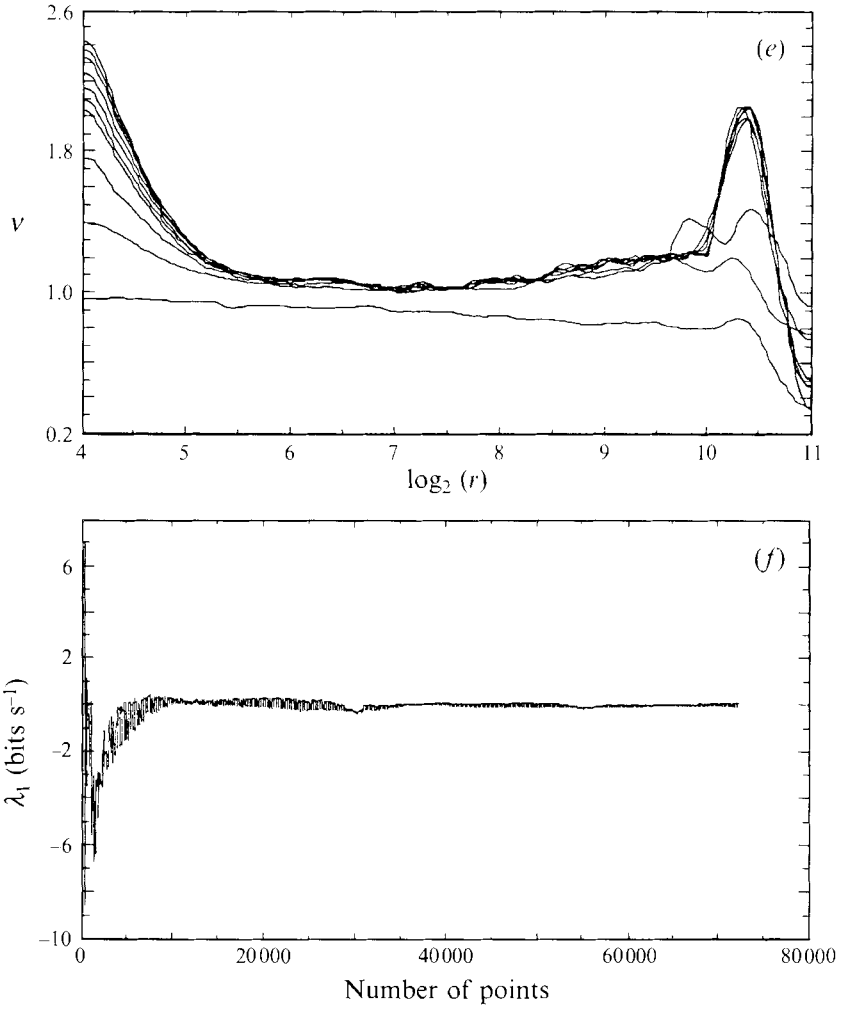

FIGURE 5. Characteristics of stable double pairing at $St_D = 1.19$, $a_f = 2.4\%$, $Re_D = 2.3 \times 10^4$, $x/D = 2.0$: (*a*) $u(t)$ signal; (*b*) power spectrum of u; (*c*) phase portrait; (*d*) Poincaré section; (*e*) correlation dimension; (*f*) largest Lyapunov exponent.

$\frac{1}{4}f_{ex}$ in SP. These presumably represent very infrequent as well as incomplete third pairings (Zaman & Hussain 1980).

The reconstructed phase portrait is seen in figure 5(*c*). As with SP, the phase portrait of SDP is a closed loop with very little scatter of the trajectories. Poincaré sections constructed at 45° and 225° (figure 5*d*) reveal two small and widely separated clusters. The standard deviations of the clusters for positive and negative crossings are 11.3 and 11.1 units respectively, while the cluster centres are separated by 1837 units. Note, again, the exclusion of parts of both axes.

From correlation dimension (figure 5*e*), it can be determined that $\nu \approx 1.07$ with scaling limits (5.15, 9.52). These limits correspond to a scaling factor of ≈ 21. Figure 5(*f*) shows the estimate of λ_1 converging to an approximate value of $\lambda_1 \approx 0.036$ b.p.s. or 5.5×10^{-4} b.p.o., again approximately zero.

Summary of periodic states The signals, spectra, Poincaré sections, dimensions (near unity) and λ_1 (near zero) indicate that these states are essentially limit cycles. The high

peak-to-noise ratios in the spectra, tight clusters in the Poincaré sections and large scaling ranges of the correlation exponents emphasize that the noise is quite small.

5. Chaotic attractors

5.1. *Quarter-harmonic chaotic attractor*

Signal and spectrum The chaotic attractor QCA has a much more irregular signal and spectrum than the periodic attractors but is nonetheless recognizable. Figure 6(*a*) shows a time trace over a period of 0.4 s which seems to be a sequence of large oscillations. Notice that, when peaks are high, their spacing corresponds to the quarter-harmonic period ($\tau_q \approx 0.015$ s), indicating that two pairings are occurring. These peaks often occur in groups of three (e.g. $t \approx 0.05$, 0.15, 0.36). At other times (e.g. $0.08 \leqslant t \leqslant 0.12$), $\frac{1}{4}f$ amplitude is low (but noticeable), and the peaks are separated by the subharmonic period, indicating single pairing with delayed (or incomplete) second pairing. Occasionally, a small peak occurs separated from the next later peak by the fundamental period. These are usually at the end of a quarter-harmonic trio and may indicate a single vortex passing without pairing.

The spectrum (figure 6*b*) is an easily recognized indicator of QCA, repeatable at many different parameter values. There is a broad peak centred at the quarter-harmonic (66 Hz) and sharp sidebands on either side of $\frac{1}{2}f_{ex}$ (132 Hz) and f_{ex} (264 Hz). The subharmonic is almost completely absent, indicating a strongly modulated amplitude. From the sharp sidebands on the subharmonic, it would seem that its modulations must be fairly periodic, whereas the broad peak at $\frac{1}{4}f_{ex}$ indicates that its modulations are not. The sharp peaks rise only 20–30 dB above the background, compared with 60–70 dB for the periodic attractors. The spectral background is broadband and falls off as frequency increases, dropping roughly 20 dB from 150 to 400 Hz. These spectral features are observed wherever QCA is found in the parameter space; for example, nearly identical spectra are seen at ($St_D \approx 1.19$, $a_f \approx 0.14\%$) and at ($St_D \approx 1.17$, $a_f \approx 22.5\%$).

Phase portrait and Poincaré sections The two-dimensional phase portrait (figure 6*c*) reveals a dense tangle of trajectories, cycling in and out of the centre as the amplitude modulates. Many projection angles were investigated to find one that revealed more structure of the attractor, but none is substantially better than the one shown. As will be shown below, this attractor has a dimension near 3 and requires an embedding dimension of 4–5; therefore, two-dimensional projections are likely to be dense and may not reveal any clear structure. The largest loops correspond to the first type of time-trace segment, where the signal amplitude is high. There are loops of intermediate amplitudes which correspond to the second type of signal segment. There are usually two loops for each quarter-harmonic period for this type, since the shape of the signal is high peak – shallow valley, low peak – deep valley. Finally, some trajectories pass very near the origin when the signal amplitude goes to nearly zero between successive modulations.

Figure 6(*d*) shows the Poincaré section of this attractor at 45° (continuous through the origin), in which some structure can be seen. The crossings are negative in the broad ridge running diagonally from (−150, −1700) to (1500, 0) and positive in the curved area running from (−1000, 1700) to (−200, 0).

Dimension and Lyapunov exponent The curves in the correlation exponent for QCA (figure 6*e*) begin to converge for embedding dimension $m \geqslant 4$. The minimum embedding dimension was determined to be $m_{min} = 4$ (see the Appendix, §A.3). Embedding dimension greater than 5 is not considered because of the heuristic

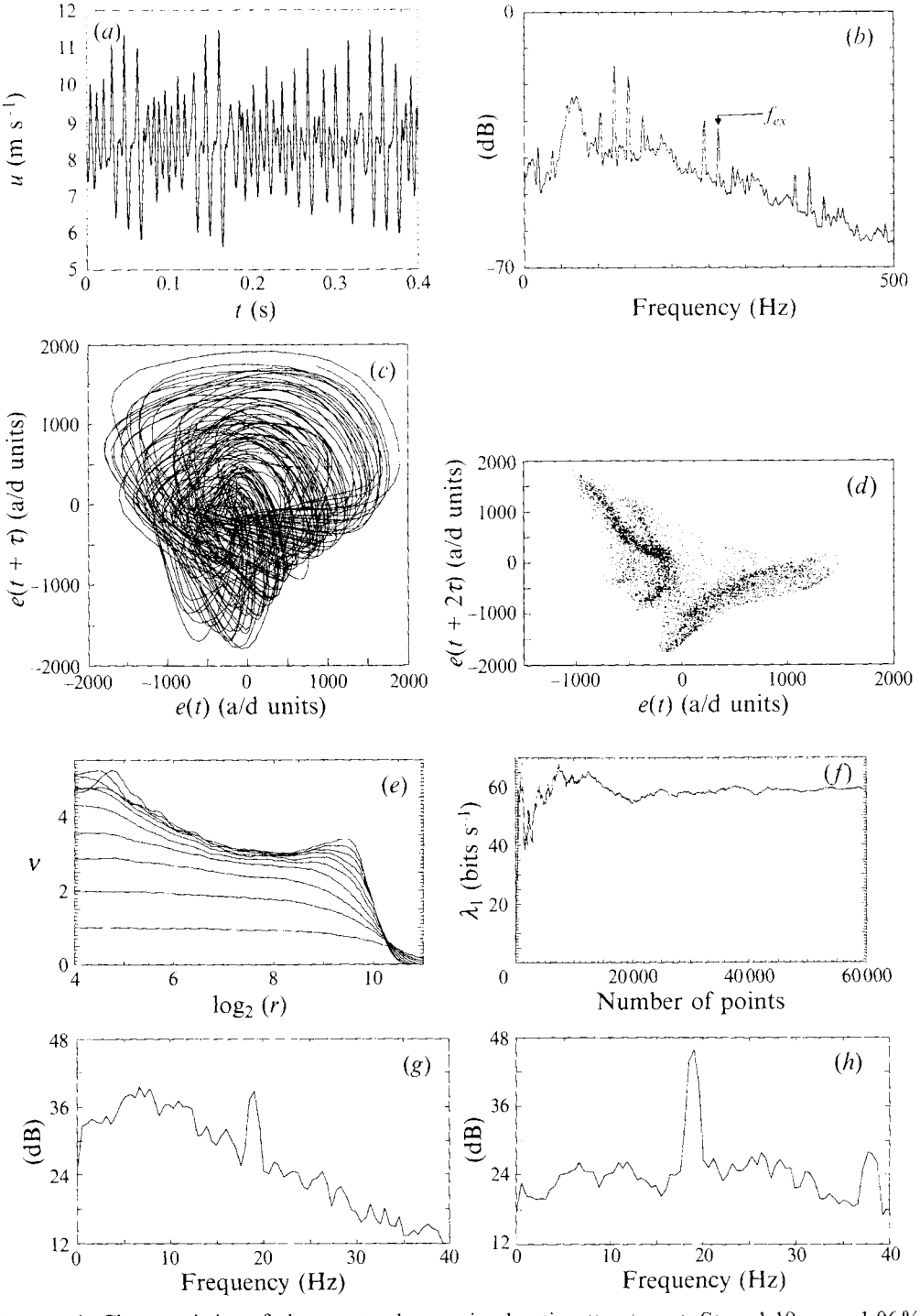

FIGURE 6. Characteristics of the quarter-harmonic chaotic attractor at $St_D = 1.19$, $a_f = 1.06\%$, $Re_D = 2.3 \times 10^4$, $x/D = 2.0$: (*a*) $u(t)$ signal; (*b*) power spectrum of u; (*c*) phase portrait; (*d*) Poincaré section; (*e*) correlation dimension; (*f*) largest Lyapunov exponent; (*g*) power spectrum of $\frac{1}{4}f_{ex}$ envelope from demodulated $u(t)$ signal; (*h*) power spectrum of $\frac{1}{2}f_{ex}$ envelope from demodulated $u(t)$ signal.

argument that the system should have no more than five dynamical variables (three amplitudes and two phase angles). For $m = 4$, $\nu \approx 2.72$ over the range $6.35 \leqslant x \leqslant 8.99$; for $m = 5$, $\nu \approx 2.83$ over the range $6.56 \leqslant x \leqslant 9.28$. One can see from this figure that the dimension estimate is not likely to exceed 3.2–3.3 regardless of the embedding dimension used. The scaling factors are between 6 and 7; while not nearly so large as those for SP (≈ 16) and SDP (≈ 21), this would still cover a range of distances of approximately 130 to 880 in the two-dimensional phase portrait (figure 6*c*).

The estimate of the largest Lyapunov exponent λ_1 is presented in figure 6(*f*). After some initial oscillations, the value has converged after 60000 points (11.4 s, 750 periods of $\frac{1}{4}f_{ex}$, ≈ 1250 orbits) to $\lambda_1 \approx 59$ b.p.s., or $\lambda_1 \approx 0.54$ b.p.o., when normalized by 4 times the reconstruction time delay (0.0091 s, between the sub- and quarter-harmonic periods 0.0076 and 0.0152 s respectively). The exponent λ_1 is positive, indicating chaos.

Spectra of amplitudes of modulating components We investigated the question as to whether the modulations of the subharmonic s and quarter-harmonic q are periodic. Two complex demodulations were performed, using $\frac{1}{4}f_{ex}$ and $\frac{1}{2}f_{ex}$ as the centre frequencies, to extract the envelopes of q and s from the signal. The low-pass filter used in the demodulation had a passband of 20 Hz and a stopband of 30 Hz, and was recursively applied to achieve 60 dB attenuation. The extracted envelopes were Fourier-analysed to determine their dominant frequencies, and the spectra are displayed in figure 6(*g*, *h*). In the spectrum of the envelope of q (figure 6*g*), there is a peak at $f \approx 19$ Hz which sits on a broadband background 10 dB down; this background rises at lower frequencies and, at $f \approx 7$ Hz, actually exceeds the amplitude of the 19 Hz peak. In contrast, the spectrum of the envelope of s (figure 6*h*) shows a peak at $f \approx 19$ Hz which is 20 dB above a background of relatively uniform amplitude. Clearly, then, the modulation of s is much more periodic than that of q.

Effect of sampling location on realizations of QCA Realizations of this attractor were sampled at many points in physical space, always with similar invariant measures. For example, samples were taken at ($St_D = 1.27$, $a_f = 1.76\%$) at half-diameter increments in x along the centreline between $0.5 \leqslant x/D \leqslant 3.5$; for all cases, ν is between 2.5 and 3.0, λ_1 is between 0.2 and 0.5 b.p.o., and Kolmogorov entropy is between 0.3 and 0.6 b.p.o. The scaling factors for $x/D = 1.5$, 2.0, 2.5, 3.0 and 3.5 are 6.0, 4.7, 2.3, 2.0 and 1.5 respectively. For $x/D \geqslant 4.0$, no scaling is observed. For $x/D \geqslant 2.5$, the probe begins to measure small-scale fluctuations, presumably because the inner edges of turbulent vortices actually pass over the probe. The low-dimensional dynamics of large-scale structures are obscured by such fine-scale motions which degrade scaling in dimension calculations. This points to the need for proper probe placement so that the global dynamics, rather than the internal dynamics of the individual vortices, are captured. Measurements should be made within the potential core (which carry smooth footprints of the vortical structures in the shear layer), rather than the turbulent vortical layer. For measurements at axial locations where this is not possible, some judiciously chosen filtering might be employed. However, the impact of various types of filtering on measures of chaos is a subject unto itself (see e.g. Mitschke, Möller & Lange 1988), and no attempt is made here to investigate that.

Occurrence of QCA in several parameter regions As mentioned above regarding the chaotic spectrum, this attractor is found in more than one region in the parameter space, both above and below SDP. Figure 3 shows a small band of chaos near ($1.1 \leqslant St_D \leqslant 1.3$, $a_f \approx 22\%$). In addition, chaos can be found at low excitation levels, although the realizations are sometimes noisy. Realizations at ($St_D = 1.19$, $a_f = 0.14\%$) show characteristics similar to the example shown in figure 6 ($St_D \approx 1.19$, $a_f = 1.06\%$): $\nu \approx 2.8$ with a scaling factor of almost 5, and $\lambda_1 \approx 0.7$ b.p.o.

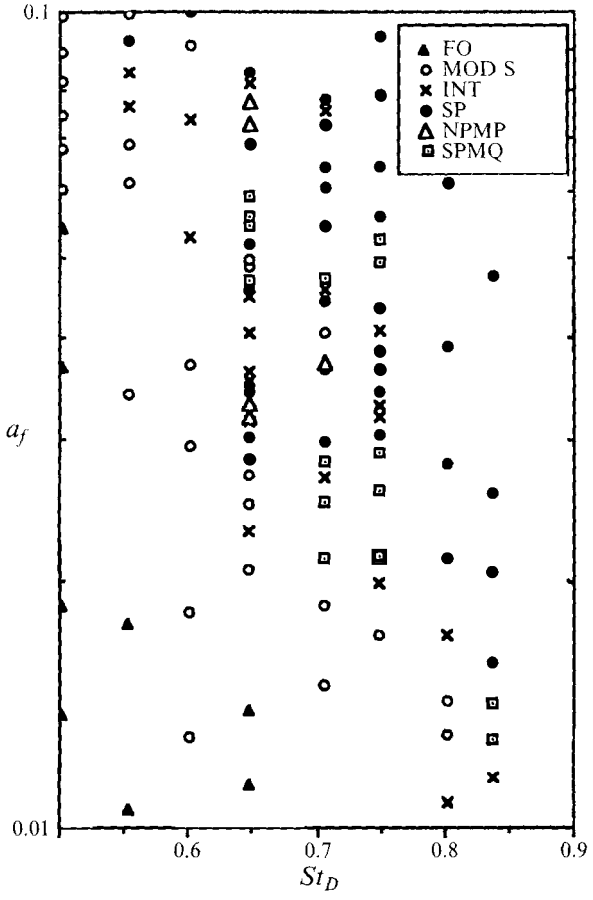

FIGURE 7. Phase diagram of the transitional jet around nearly periodic modulations of pairing.

Summary The characteristics presented here (spectral broadening and filling, $\nu > 2$, $\lambda_1 > 0$) indicate that QCA is indeed a chaotic attractor that results from non-periodic modulations, particularly of the quarter-harmonic. Its persistence at different spatial locations as well as in different regions of the parameter space indicates that QCA is not a chance occurrence but is instead an intrinsic part of the dynamics of this system.

5.2. *Nearly periodic modulations of pairing*

Local phase diagram Figure 7 shows the phase diagram for the region bounded by ($0.5 \leqslant St_D \leqslant 0.85$, $0.01 \leqslant a_f \leqslant 0.10$), in which several different states can be distinguished: fundamental only (FO), stable pairing (SP), aperiodic modulations of $\frac{1}{2}f$ (MOD S), nearly periodic modulations of pairing (NPMP), and stable pairing with modulated quarterharmonic (SPMQ). SP is the dominant state in this diagram for higher St_D and a_f (upper right), while FO dominates at the lower St_D and a_f (lower left). In between are seen SPMQ, MOD S and NPMP, with some intermittency. The most remarkable feature is the relatively dense intermingling of states occurring in the central region, where changes of a fraction of a percent in a_f lead to several changes of state. For example, at ($St_D = 0.65$, $2.8\% \leqslant a_f \leqslant 5\%$), the state changes from MOD S to SP to NPMP to SP to MOD S to SP to SPMQ.

Signal and spectrum In this region, we focused our attention on NPMP, seen in figure 7 at ($St_D = 0.65$, $a_f = 3.2$, 3.3, 7.3 and 7.8%), and at ($St_D = 0.71$, $a_f = 3.7\%$ and

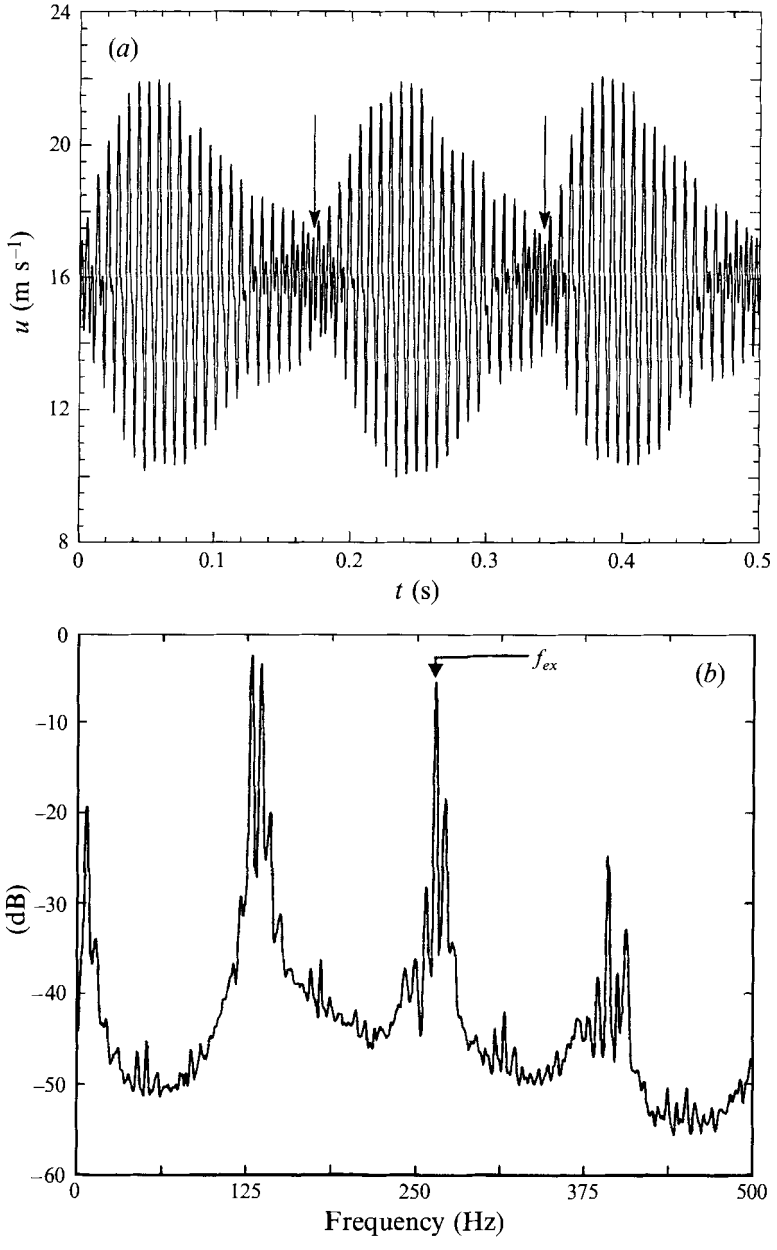

FIGURE 8. (*a*) Signal $u(t)$ and (*b*) power spectrum of u for nearly periodic modulations of pairing at $St_D = 0.68$, $a_f = 3.40\%$, $Re_D = 4.0 \times 10^4$, $x/D = 2.0$.

7.4%). It is of interest because (i) it is the only evidence of nearly quasi-periodic flow in this system and reveals interesting attractor structure, and (ii) it offers an opportunity to investigate the transition scenario (to be addressed in a future paper). Figure 8(*a*) shows a representative time trace of NPMP. Each modulation is somewhat different from the rest; the period of modulation, the envelope shape and the waveform at various stages of the modulation are similar but not exactly the same. This signal corresponds to 0.5 s (66 periods of $\frac{1}{2}f$) and contains almost 3 periods of the modulation, each containing approximately 22 periods of the subharmonic. The amplitude

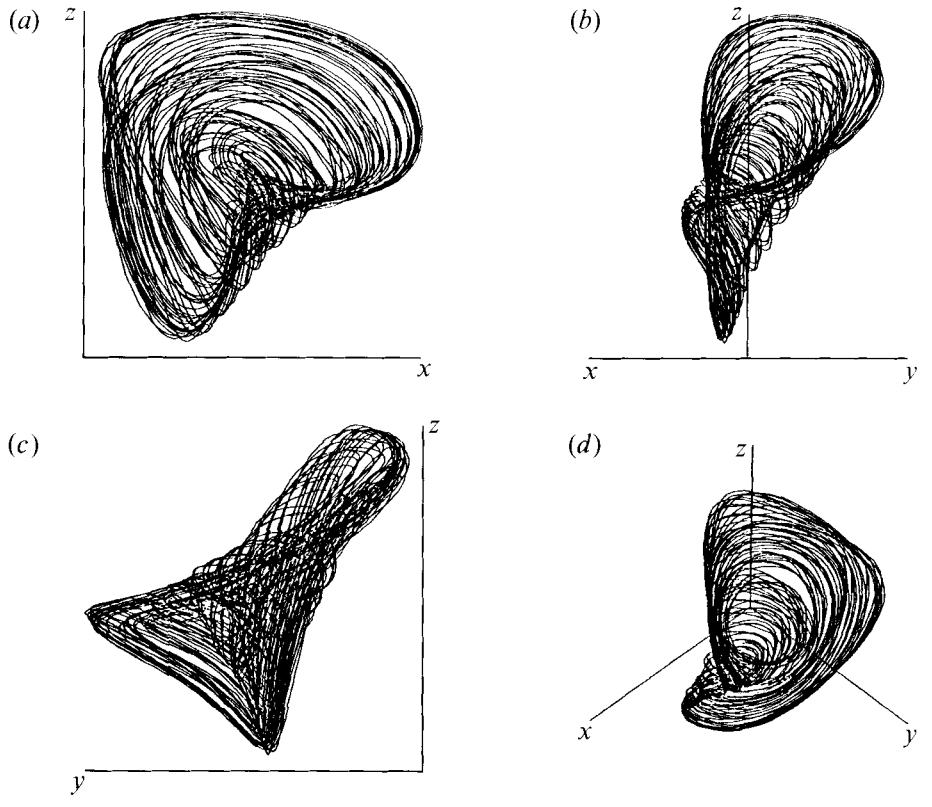

FIGURE 9. Phase portraits of nearly periodic modulations of pairing at $St_D = 0.68$, $a_f = 3.40\%$, $Re_D = 4.0 \times 10^4$, $x/D = 2.0$: (*a*) $\phi = 0°$, $\theta = 0°$; (*b*) $\phi = 0°$, $\theta = 45°$; (*c*) $\phi = 0°$, $\theta = 90°$; (*d*) $\phi = 45°$, $\theta = 45°$.

variations indicate that the pairing location is shifting up- and downstream almost periodically. Furthermore, at the minimum amplitude point between the modulation wavepackets, the phase shifts by π. This can be seen by tracing pairs of peaks (first large, then small) as the envelope diminishes. There is always one first peak with no smaller peak after it (as indicated by arrows in figure 8*a*), denoting the phase shift. Since the subharmonic period is equivalent to 2π, a π phase shift indicates that a single vortex escapes pairing at the end of each modulation period.

The signal is quite similar to that observed by Husain & Hussain (1989) in their detuned excitation study in a mixing layer. In their experiments, they controlled both fundamental and a detuned subharmonic (f and $\frac{1}{2}f \pm \Delta f$) to produce periodic modulation of subharmonic amplitude. In the present experiments, however, controlled forcing is only at the fundamental, and the subharmonic is *self-modulating via feedback*. Corresponding to this, the spectrum (figure 8*b*) shows twin peaks (plus additional harmonics of the modulation) on either side of the subharmonic frequency ($\frac{1}{2}f_{ex} = 132$ Hz); the spectral power at $\frac{1}{2}f_{ex}$ is actually 25 dB below the sidebands. There is a low-frequency peak, with two harmonics, at $f \approx 7$ Hz corresponding to the modulation frequency. The peaks are slightly broadened, but the spectrum is not filled between peaks, with valleys 40 dB or more down from the peaks.

Phase portraits and Poincaré sections Figure 9 shows a phase portrait viewed from four different projection angles, used to reveal as much of the attractor structure as

possible and to identify a 'better' viewing angle for exploration of the structure. Rather than reconstructing in two dimensions using only $(e(t), e(t+\tau))$, these are reconstructed in three-dimensional space $(e(t), e(t+\tau), e(t+2\tau))$, rotated to selected viewing angles and viewed from far away along rays defined by their polar and azimuthal angles ϕ and θ respectively (identified in the figure caption). Since there are only three dynamical variables (two amplitudes and a phase difference), the attractor should be fully revealed in three dimensions; this was confirmed by computing the minimum embedding dimension. Figure 9(*a*) is equivalent to the usual two-dimensional phase portrait ($\phi = 0°$, $\theta = 0°$). Trajectories can be seen looping into and out of a small folded region near the centre, with the amplitude of each loop determined by the modulating envelope (see figure 8*a*). The attractor looks drastically different in a view along the ($\phi = 0°$, $\theta = 45°$) line (figure 9*b*); it appears as if it might be a hollow cylinder or 'funnel', fluted open at the upper end with trajectories forming bundles as they cross in an x pattern in the front, but flaring out as they loop around the back. Along the ($\phi = 0°$, $\theta = 90°$) line (figure 9*c*), the view gives the impression that the motion is not necessarily in planes but may form a tubular shape (see discussion of the Poincaré section below). Other views at $\phi = 0°$ (e.g. $\theta = 135°$ or 180°) show nothing particularly revealing and are not shown. Finally, figure 9(*d*) shows a view along $\phi = 45°$, $\theta = 45°$, which is figure 9(*b*) tilted forward by 45°, looking down into the funnel; it reveals no opening, as one might expect from viewing figure 9(*a–c*). While these four views do not reveal the attractor totally, they together give a much better perception of the attractor than a single two-dimensional projection does.

The Poincaré section (figure 10*a*) was made by cutting the reconstructed attractor in figure 9(*d*) with a plane normal to the page and aligned with the z-axis. This reveals two open loops, verifying that the shape in figure 9(*c*) is indeed a hollow tube similar to a torus. It is not clear from figure 10(*a*) whether the scatter in the Poincaré section is due to noise or chaos; features such as the ones near $(x, y) \approx (-500, 500)$ and $(-1000, 900)$, as well as in the region $(600 \leqslant x \leqslant 1300, y \approx -100)$, look like folds and accumulation points which might be associated with the breakup of a torus in a three-frequency route to chaos.

Dimension and Lyapunov exponent: quasi-periodicity and chaos? NPMP has both quasi-periodic and chaotic characteristics. Calculation of the correlation exponent (done for a number of data sets) typically shows two scaling regions (e.g. see figure 10*b*). The meaning of the two regions is not obvious; it might imply slightly different scaling exponents, and perhaps different dynamics, at different scales. Based on this hypothesis, λ_1 values were calculated separately at these two scales, being usually positive at smaller scales but approximately zero at larger scales. These results are presented and discussed below.

The correlation exponent for data at ($St_D = 0.68$, $a_f = 3.4\%$) is shown in figure 10(*b*). For embedding dimension $m \geqslant 4$, a peak develops separating two regions with slightly different values of ν: higher at smaller scales in phase space than at larger scales. Local averages at $x \approx 7$ (recall $x \equiv \log_2 r$; r is distance in phase space) yield $\nu \approx 2.1$ for $m = 3$ and $\nu \approx 2.3$–2.4 for $m = 4$; local averages at $x \approx 8.5$ yield $\nu \approx 1.9$–2.0 for $m = 3$ and $\nu \approx 2.3$ for $m = 4$. This difference (0.3–0.4) between ν in the two scaling regions is less than that (up to 0.5–0.8) for other data sets taken from this region of the parameter space. Typically, the region at smaller x has higher ν, ranging up to $\nu = 2.8$, while in the higher-x region ν may fall to as low as 2.0. This separation into two regions does not appear to be an error in the estimator for the following reasons: (i) it does not appear in calculations for data from other states; (ii) it appears in almost every set of NPMP data; and (iii) the point-skipping correction of Theiler (1986) was employed (to

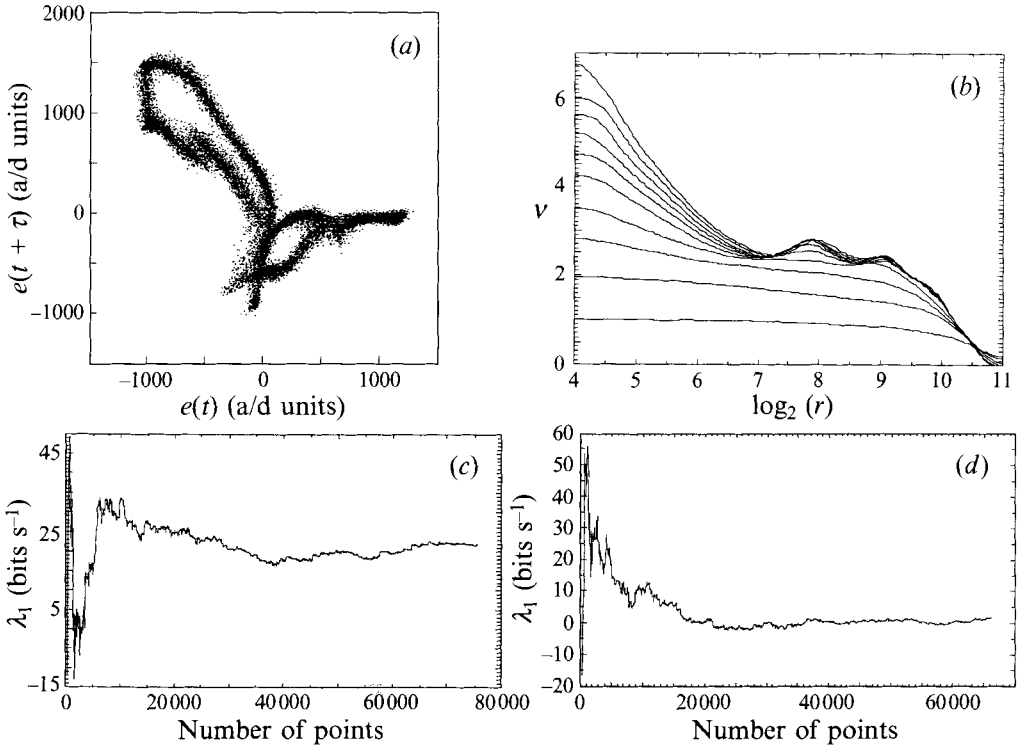

FIGURE 10. Characteristics of nearly periodic modulations of pairing at $St_D = 0.68$, $a_f = 3.40\%$, $Re_D = 4.0 \times 10^4$, $x/D = 2.0$: (*a*) Poincaré section; (*b*) correlation dimension; (*c*) largest Lyapunov exponent at small scales; (*d*) largest Lyapunov exponent at large scales.

	Scaling limits				
m	low x	high x	λ_1 (b.p.s.)	λ_1 (b.p.o.) (4τ norm)	λ_1 (b.p.o.) ($\frac{1}{2}f_{ex}$ norm)
3	6.8	8.3	22	0.25	0.17
3	8.2	9.0	1.5	0.017	0.012
4	6.7	8.0	4.3	0.049	0.033
4	8.0	9.0	0.63	0.0071	0.0048

TABLE 1. Largest Lyapunov exponent for NPMP; $St_D = 0.68$, $a_f = 3.4\%$, $Re_D = 4.0 \times 10^4$, $x/D = 2$.

an extreme, skipping 10^3 points $\approx$ 20 orbits out of 10^6 points). The Theiler correction ensures that there is no temporal correlation between points in the dimension calculation, which often leads to oscillations in the correlation exponent. Nonetheless, these two regions persist.

The estimates for λ_1 at $m = 3$ for this case ($St_D = 0.68$, $a_f = 3.4\%$) are seen in figure 10(*c*, *d*), and for $m = 3$ and 4 in table 1. (A calculation of minimum embedding dimension showed that $m = 3$ suffices.) At small scales in phase space, there is quite a difference between λ_1 at $m = 3$ and $m = 4$ (0.25 and 0.049 b.p.o. respectively), but both are clearly positive. At large scales in phase space, however, the λ_1 values are roughly an order of magnitude smaller in both embedding dimensions (0.017 and 0.0071 b.p.o.); as mentioned in §4.1, these values are probably zero to within the margin of error. For

other NPMP data sets sampled, typically $0.1 \leqslant \lambda_1 \leqslant 0.5$ b.p.o. for small x and $\lambda_1 \approx 0$ for large x (although $\lambda_1 > 0$ for both regions in some cases). Results for λ_1 were confirmed with the Kruel–Eiswirth algorithm (Th.-M. Kruel & M. Eiswirth 1992, personal communication).

These results seem to indicate regular behaviour at large scales in phase space but chaotic behaviour at small scales. This is consistent with the Poincaré section, which shows a loop structure at large scales but with local folds and accumulation points and possible additional small-scale structure. Converting the scaling limits for this case into actual distances in dimension 2, one finds that the ranges are approximately 160–430 units (i.e. integer levels of the 12-bit a/d converter) for the chaotic region and 430–720 units for the regular (approximately quasi-periodic) region. Looking at the Poincaré section (figure 10*a*), the smallest chaotic scale (160 units) approximates the thickness of the bands that make up the loops, while the largest regular scale (720 units) encompasses roughly one quarter of the maximum spatial extent of the section and is close to the standard deviation σ (653 units) of the time series data set; σ is a good measure for the reconstructed attractor size. The intermediate scale (430 units) roughly corresponds to the distance across the openings in the loops. If these correspondences have physical significance, then the scenario might be as follows: (i) for scales smaller than the thickness of the bands, the distribution of crossings is essentially random; (ii) for scales larger than the band thickness but smaller than the loops themselves, fractal scaling and chaotic behaviour is seen; and (iii) for larger scales up to the size of the attractor, regular scaling ($\nu \approx 2$) and regular (viz., approximately quasi-periodic) behaviour is seen. Does this mean the attractor is both quasi-periodic and chaotic? Not necessarily; it may just be an artifact of the data analysis tools employed, particularly the Wolf algorithm for λ_1, which is rather scale-sensitive. However, it is quite probable that this dual nature would be seen in *any* attractor that is chaotic but close to quasi-periodicity. Therefore, the best characterization of *NPMP is that it is a chaotic attractor that has quasi-periodic features at coarse resolution.*

6. Other states

6.1. *Fundamental only*

In figure 3(*b*), there is a large 'fundamental only' (FO) region which occupies much of the diagram at lower St_D and a_f. (Our experiments show that it can extend at least as low as $St_D = 0.25$.) Within this region is the 'preferred mode' (Hussain & Zaman 1981), defined by the St_D (≈ 0.3–0.4) producing maximal amplification of an axisymmetric fundamental disturbance; generation of subharmonics in this mode is negligible.

Figure 11(*a*) shows a typical time trace for FO sampled at ($St_D = 0.40$, $a_f = 1.0\,\%$). FO is not nearly so periodic as the time traces of SP and SDP. The fundamental period is easily distinguished, but the waveform in each period is different from the others; there is a great deal of 'jitter' (i.e. non-uniformity) in the signal. At no point in the parameter space was a periodic signal observed for this state. In the spectrum for FO (figure 11*b*) at this point in the parameter space, the peak at the forcing frequency is sharp, but is only 25 dB above the background, compared to about 70 dB for SP and SDP. The spectral background is a high pedestal which is nearly constant between the fundamental and first harmonic, and falls off rapidly at higher frequencies. The peak frequency of the background pedestal does not remain fixed relative to the fundamental when St_D is changed slightly; the pedestal St_D (based on the peak frequency of the hump other than f_{ex} and its harmonics) appears to remain approximately constant

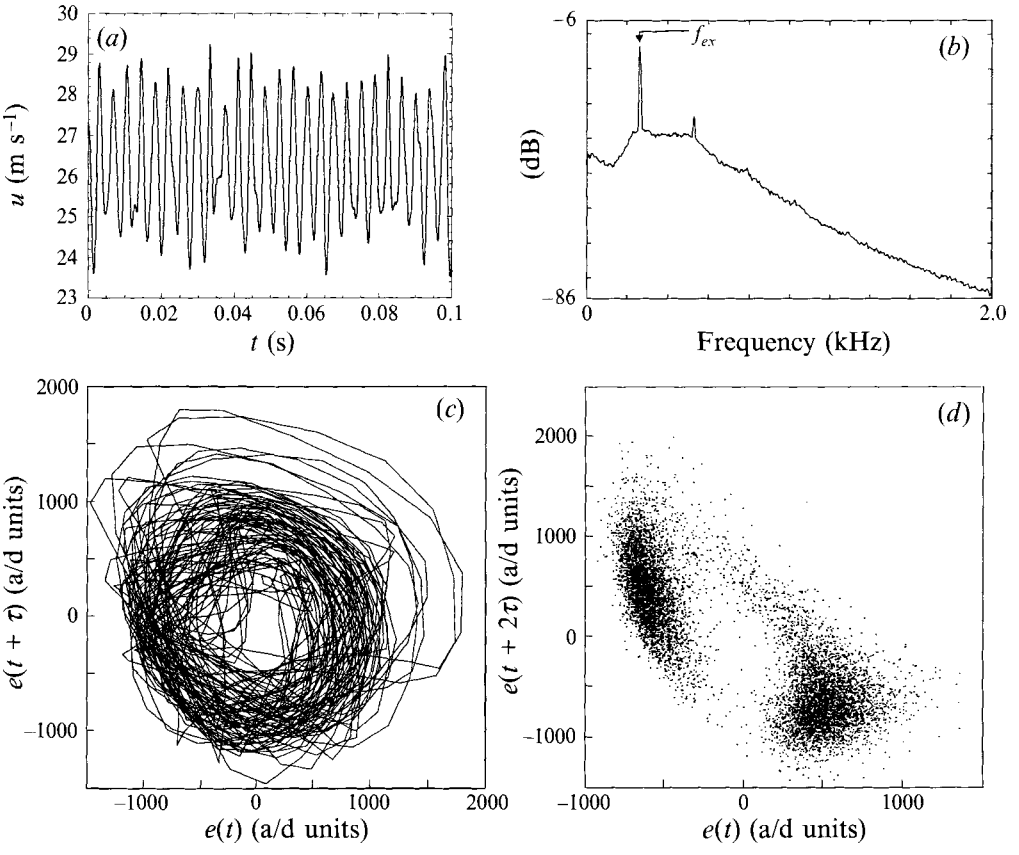

FIGURE 11. Characteristics of fundamental only at $St_D = 0.40$, $a_f = 1.00\,\%$, $Re_D = 6.9 \times 10^4$, $x/D = 1.5$; (*a*) $u(t)$ signal; (*b*) power spectrum of u; (*c*) phase portrait; (*d*) Poincaré section.

regardless of the excitation St_D. This indicates dynamics that are independent of the excitation; indeed, in the absence of any periodic forcing, a spectral peak is seen which corresponds to $St_D = 0.4$. Many have speculated that this is due to natural feedback from vortex rollup itself. While this may be true, no computation using data from unexcited jets in our lab has ever revealed measurable dimension, even using up to 5×10^6 data points (i.e. more than 10^5 attractor orbits). The broadband receptivity of the jet instability is most likely responsible for the pedestal, regardless of feedback dynamics.

The phase portrait for FO at ($St_D = 0.40$, $a_f = 1.0\,\%$) has the appearance of either a very noisy limit cycle or perhaps a torus (figure 11*c*). Figure 11(*d*) shows Poincaré sections at 45°; unlike the sections of SP and SDP, the clusters of positive and negative crossings are very diffuse. There is no evidence of an open loop in either the positive or negative crossings, ruling out the possibility of a torus (and hence quasi-periodicity).

The correlation exponent (not shown) has very poor scaling; in embedding dimension $m = 3$, $\nu \approx 1.5$ with a scaling factor of only about 2. Since the scaling region is small, we looked for higher dimension at other scales; however, no other scaling is seen for $m \leqslant 10$. The Lyapunov exponent λ_1 (not shown) is more surprising; it is negative: $\lambda_1 \approx -14$ b.p.s. (-0.06 b.p.o.)! However, in tests using the Wolf algorithm with inputs from the ν scaling region, we have found that a noise-contaminated sine wave can exhibit a small negative λ_1; we term this 'noisy periodicity'. This phenomenon

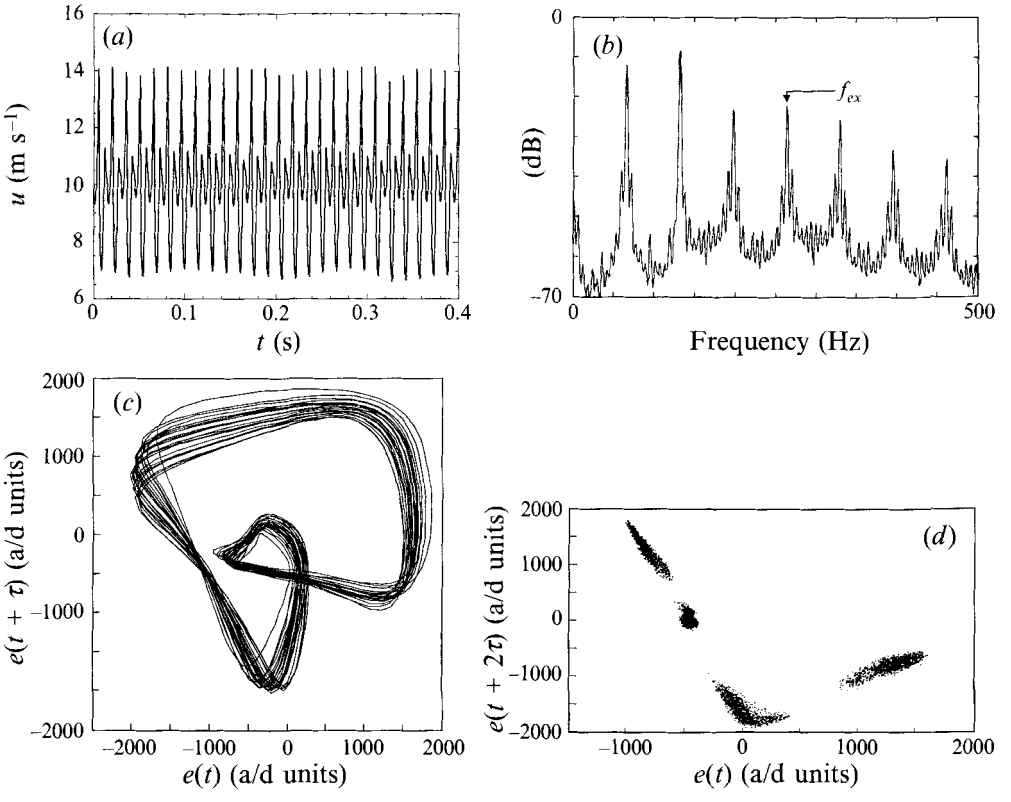

FIGURE 12. Characteristics of stable pairing with modulated quarter-harmonic at $St_D = 1.00$, $a_f = 0.48\%$, $Re_D = 2.7 \times 10^4$, $x/D = 2.0$: (*a*) $u(t)$ signal; (*b*) power spectrum of u; (*c*) phase portrait; (*d*) Poincaré section.

(i.e. $\lambda_1 < 0$) is presumably an artifact of the algorithm itself, since a sine wave (i.e. limit cycle) should have $\lambda_1 = 0$ and noise should have $\lambda_1 > 0$.

6.2. *Stable pairing with modulated quarter-harmonic*

Between SP and SDP in the phase diagram (and other locations as well), a state (SPMQ) is observed in which the subharmonic is stable and strong (as observed in the instantaneous spectrum), but the quarter-harmonic is modulated and weaker than for SDP. The presumption here, not verified by educed spatial vorticity patterns, is that the first pairing is periodic, but the second is not and modulates aperiodically. A time trace of this state (figure 12*a*) shows that the amplitude is fairly constant with a weak modulation; although this particular realization has fairly periodic modulations, such is not always the case. A frequency spectrum of SPMQ is shown in figure 12(*b*). The $\frac{1}{4}f_{ex}$ peak is about 5 dB lower than $\frac{1}{2}f_{ex}$, and there are modulation sidebands on either side about 25 dB down. There are also sidebands near the base of the $\frac{1}{2}f_{ex}$ peak, but these are weaker than those around $\frac{1}{4}f_{ex}$. If the modulations were less periodic, the sidebands would be more smeared with a resultant peak broadening, particularly of $\frac{1}{4}f_{ex}$.

A phase portrait (figure 12*c*) reveals a double-loop structure, consistent with the shape of the time trace: large peak–shallow valley, small peak–deep valley. The spread of trajectory bundles is much more than in SP or SDP owing to the larger modulation

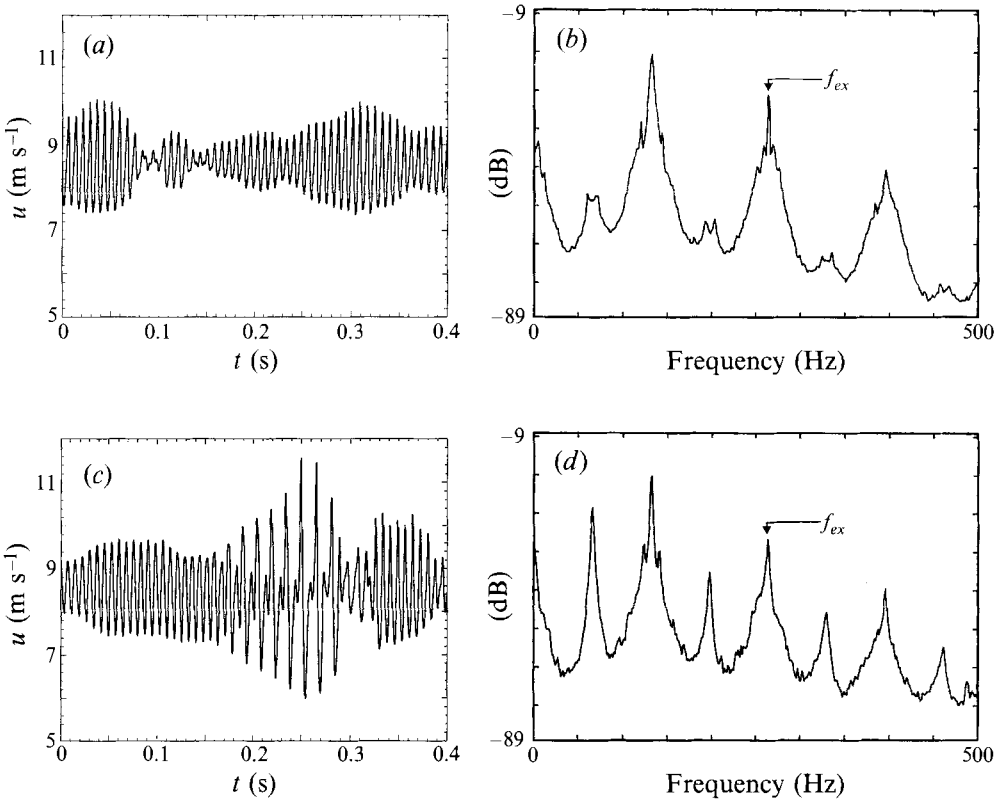

FIGURE 13. Characteristics of aperiodic modulations at $St_D = 1.19$, $a_f = 0.30\%$, $Re_D = 2.3 \times 10^4$, $x/D = 2.0$: (*a*) $u(t)$ signal; (*b*) power spectrum of u; and at $St_D = 1.19$, $a_f = 0.54\%$, $x/D = 2.0$: (*c*) $u(t)$ signal; (*d*) power spectrum of u.

of the envelope. Based on the signal and phase portrait, one might expect the modulation to appear as open loops (like a torus) in the Poincaré sections (in the 45° planes; figure 12*d*), but this is not the case, thus eliminating any expectation of quasi-periodicity.

The correlation exponent (not shown) has a narrow scaling region near $x \approx 8.5$ in which $\nu \approx 1.3$ for $m = 3$ with a scaling factor of less than 3. Again, as in FO, $\lambda_1 < 0$. The only similarity between SPMQ and FO is that their signals appear to be periodic with an aperiodic component superimposed. Unlike FO, the aperiodic component in SPMQ appears to be somewhat organized. Nonetheless, both cases reveal similar results: $1 < \nu < 2$ and $\lambda_1 < 0$.

6.3. *Aperiodic modulations*

The label 'aperiodic modulations' covers a variety of states with modulated velocity traces and spectra with peaks (at $\frac{1}{4}f_{ex}$ or $\frac{1}{2}f_{ex}$, and harmonics) broadened to varying degrees. Figure 13 shows time traces and spectra of two cases in this category, both captured at $St_D = 1.19$. In the first case ($a_f = 0.30\%$; figure 13*a*), one sees a modulated signal which appears to have a single 'carrier' frequency ($\frac{1}{2}f_{ex}$); longer realizations reveal that the modulation envelope has no recognizable shape or repeated feature. There are large, broad peaks in its spectrum, centred at $\frac{1}{2}f_{ex}$ and its harmonics, with small sidebands around these peaks (figure 13*b*); much weaker, broad peaks are found

at $\frac{1}{4}f_{ex}$ and its odd harmonics. The time trace and spectrum apparently indicate vortices whose pairing locations fluctuate aperiodically (or, occasionally, they do not pair), as well as infrequent and/or incomplete second pairings. By comparison, the second time trace (for $a_f = 0.54\%$; figure 13*c*) reveals the quarter-harmonic (for $0.17 \lesssim t \lesssim 0.29$), which appears intermittently in longer realizations. The corresponding spectrum (figure 13*d*) shows significantly more quarter-harmonic than in figure 13(*b*), the $\frac{1}{4}f_{ex}$ peak being only 10 dB (compared with 40 dB) down from the $\frac{1}{2}f_{ex}$ peak. While similar to the first case ($a_f = 0.30\%$), the time trace and spectrum suggest that second pairings occur more frequently in this case.

The point of these observations is that while frequent pairings (and less frequent second pairings) occur in AM, there is no obvious pattern (e.g. nearly periodic amplitude modulations or periodic appearance of the quarter-harmonic). Behaviour similar to these two cases is seen at many other points in the parameter space. All their signals have seemingly random modulations and a non-stationary appearance; the signal amplitude, shape of the amplitude modulation envelope and/or dominant frequency vary in time but may remain the same for long periods of time before each change. All spectra for AM have peaks at $\frac{1}{4}f_{ex}$ or $\frac{1}{2}f_{ex}$ (or both) which broaden at their bases without the strong, distinctive sidebands seen in QCA and NPMP. While the relatively sharp spectral peaks with fairly low background might suggest low-dimensional dynamics, signal analysis for chaos in AM has revealed little; realizations were taken for many parameter values and analysed for ν and λ_1 with no definitive results. For some realizations, the correlation integral has no scaling region; for others, a small scaling region is found where $1.0 \leqslant \nu \leqslant 1.5$, and $\lambda_1 \approx 0$ or perhaps even slightly negative.

6.4. *Why is chaos not measurable for FO, SPMQ or AM?*

As has been discussed briefly in §§6.1–6.3, these states show a puzzling lack of scaling in dimension calculations or negative largest Lyapunov exponents. While we do not yet have an answer to this question, we do have several hypotheses which may explain one or more cases; the first three relate to lack of scaling and the last two relate to negative Lyapunov exponents. These five possibilities are enumerated below.

Intermittencies? In the AM regions, it is likely that there are many different states close to each other in the parameter space, as was seen in figure 7 for the region around NPMP. (We devised simple iterative map models of pairing which exhibit densely packed states as well.) If this is the case, the non-stationary nature of the signals, the lack of scaling, etc., in signal analyses may be due to intermittency, i.e. the alternation of the system between two (or more) states. If two intermittent states are sampled, the reconstruction of any 'attractor' may exhibit no scaling (although scaling is possible; this will be described in a future paper). These intermittencies can naturally occur if the parameters are set on the boundary between two states, or they could be due to small parameter drift. If the states were dense in the parameter space, only very slight drifts would be necessary.

Non-axisymmetric vortex dynamics? During simultaneous velocity measurement and flow visualization in a low-Re_D water jet, Berger (1993) observed modes (near SDP in parameter space but at lower a_f) consisting of intermittent switching between axisymmetric and tilting modes (including crosslinking of vortices with both their upstream and downstream neighbours simultaneously). The time traces for this state were quite similar to those seen for AM in the present experiments (e.g. figure 13), suggesting that intermittent tilting may occur for AM. The origin and dynamics of tilting modes are unknown and may be high-dimensional or even noise-driven.

High-dimensional chaos? It has been seen that periodic forcing at particular

frequencies and amplitudes can lead to low-dimensional, deterministic behaviour. However, even if the flow is deterministic, there is no guarantee that the behaviour will be low-dimensional. Our lack of ability to estimate ν and λ_1 could be due to the fact that the dynamics has high dimension. Ruelle (1990) estimated that the number of points N_ν necessary to calculate dimension should scale as $N_\nu \sim \rho^{-d/2}$, where ρ is the ratio of the minimum scaling size to the size of the attractor (i.e. approximately the inverse of the scaling factor in a dimension calculation) and d is the attractor dimension. For Lyapunov exponents, he estimated $N_\lambda \sim \rho^{-d}$. If these states are high-dimensional, it is quite possible that their dimension could not be estimated using the moderate sample lengths we used.

Convective chaos? Deissler & Kaneko (1987) defined chaos in convectively unstable flows as the divergence of similar initial states measured in an advecting frame. Their tests showed negative λ_1 using data from a stationary frame but positive λ_1 in a frame advecting at the group velocity of the most unstable mode. Since this flow is locally convectively unstable, this is an appealing explanation for negative λ_1. However, low-dimensional temporal dynamics (viz., periodic and chaotic states) are evidence that global modes exist (see §§2.1–2.3) that can be characterized using data from a single stationary probe. Convective chaos might be expected when the resonance is broken, due to strong noise or weak feedback, but this is not the case here. For example, SPMQ is observed even at $a_f > 10\%$, whereas deterministic temporal states can be seen at $a_f \approx 1\%$ (figure 3*b*); why would noise be more dominant or feedback weaker in the former case than in the latter?

Noisy periodicity? As pointed out in §6.1, a noise-contaminated sine wave can appear to have $\lambda_1 < 0$ using the correlation dimension/Wolf algorithms; we call this 'noisy periodicity'. The reason for this has not been discovered, but it opens up the possibility that the dominant feature may be periodic with superposed high-dimensional chaotic fluctuations (which have the same effects on the calculations as noise). These fluctuations would limit the scaling region of the (one-dimensional) periodic fluctuations in the correlation exponent calculation and would also increase the estimate of dimension. If λ_1 is calculated at the scales (in phase space) of the periodic motion, one expects $\lambda_1 = 0$. This seems to occur in some cases of AM, but in other cases of AM, as well as SPMQ and FO, $\lambda_1 < 0$. This raises a question as to whether the negative λ_1 is due to the flow or the algorithm; no answer has been found yet.

7. Concluding remarks

The application of dynamical systems techniques to transitional jet flows has been successful in this study, since well-characterized attractors have been found, occupying sizeable regions of the parameter space. Our conceptual model of the jet dynamics is supported by experimental evidence: the measured effects of feedback on exit phase difference ϕ, the strong self-modulation of the chaotic attractors and aperiodically modulated states (due to variations in ϕ, discussed more in a future paper), and global modes as indicated by temporal attractors, measurable over a range of locations in physical space. Clearly, the forced transitional jet behaves as a dynamical system.

We have proposed a definition that distinguishes between physically and dynamically open flows. Although this distinction is obvious in some ways, the point must be made that a flow being physically open does not mandate it to be dynamically open; this question is related to the nature of its instability rather than necessarily its physical boundaries. Even in the case of convective instability (which makes a flow dynamically open), global modes can occur via feedback (which renders the dynamics closed).

Global modes – a concept not new in this research – are clearly found due to feedback from volume sources, i.e. vortex pairings (as suggested by Huerre & Monkewitz 1990), rather than boundary sources such as downstream obstacles.

What does the presence of periodicity and chaos say about the vortex dynamics in transition? Since the fundamental is being forced, each vortex rollup occurs at approximately the same saturation amplitude and location. However, the evolution of subharmonics, leading to vortex pairings, is not forced but only indirectly controlled. Obviously, exact periodicity of signals implies that the evolution of each pair of vortices (or pair of pairs in the case of SDP) goes through exactly the same sequence of events as the pair(s) before. In the chaotic cases (NPMP and QCA, the interactions can range from complete pairing to no pairing at all, depending on the initial amplitudes and phase differences of the fundamental, subharmonic and quarter-harmonic. The interactions differ from pair to pair, but feedback enables the interaction of one pair to influence the next pair, and so on. The presence of periodicity and temporal chaos, simply put, means that the long-time sequence of two-dimensional vortex interactions is deterministic, owing to feedback, rather than noise-driven.

What is the spatial extent of this dynamical system? Clearly, owing to breakdown, it will not persist far beyond the end of the jet potential core. The precise distance, however, will depend on where two-dimensional instabilities cease to dominate; this depends on the state of the system. For example, SP shows only one well-organized vortex pairing; SDP, involving two pairings, should continue further in space than SP. This is supported by the phase-averaged vorticity contours of SP and SDP from Bridges & Hussain (1992), which show organized vortical motions as far as perhaps $x/D \approx 4$ for SP and beyond $x/D \approx 5$ for SDP. Centreline-amplitude measurements show that the quarter-harmonic reaches its peak near $x/D \approx 3$ for SDP but not until $x/D \approx 4$–5 for QCA; time-averaged two-dimensional measurements show that significant hydrodynamic features (such as Reynolds stress) differ for SDP and QCA up to $x/D \approx 6$–8. In most cases, then, the dynamical system is not expected to extend beyond about 10 diameters.

Can dynamical systems techniques be applied to more complex geometries and more turbulent domains than this (near field of an initially laminar) jet, or even in dynamically open flows? While the outlook is not good, dynamically closed behaviour in this physically open shear flow means that the answer to the first question might be a qualified yes. However, the estimate of a high dimension (> 700) in a low-Re turbulent channel flow (Keefe, Moin & Kim 1992) indicates that the approach, even if applicable, may be of limited utility. In order to describe such a flow, a large number of model equations would need to be developed; in comparison, direct numerical simulation (DNS) would require a larger number of equations but having a more straightforward derivation (e.g. spectral or finite-difference representations of the Navier–Stokes equations). However, even DNS suffers in physically open flows from the combined effect of convective instabilities with artificially imposed outflow boundary conditions. As to the question of dynamically open flows, less is known. While Deissler & Kaneko (1987) have defined convective chaos, implying determinism in an appropriately moving frame, the ability to model or measure this phenomenon in laboratory flows is currently beyond our grasp. The techniques currently used in spatiotemporal chaos, such as spatial correlations and coherence functions, may have little meaning when the flow is convectively unstable, since fluctuations will advect through any arbitrary finite boundaries, leaving no imprint on the future of the flow in the absence of global modes. Therefore, the exploitation of global modes in physically open flows is an attractive avenue for studying and controlling the flow

evolution; concurrently, techniques should be pursued to characterize and model open flows in general.

Transitions between these attractors will be addressed in a future paper. Intermittency via tangent bifurcations is the only observed route to chaos. A local investigation near the SDP–QCA transition reveals hysteresis and the formation of an isolated branch for QCA not reachable by smooth parameter changes. Notably absent, however, is any clear evidence of period-doubling or Hopf bifurcations.

The authors are grateful to Bill Berger for performing many of the phase diagram experiments and for figure preparation and to Satish Narayanan for a careful review of the manuscript. This work was supported by the Office of Naval Research grant N00014-89-J-1361.

Appendix. Experimental facilities and procedures

A.1. *Facility and equipment*

The experiments reported herein were performed in the aeroacoustic jet facility in the anechoic chamber in the University of Houston Mechanical Engineering Department, which is extensively documented in Bridges & Hussain (1992). The overall layout is shown in figure 14 and is described below; letters in parentheses refer to those in the figure. The chamber (K) is a ventilated and air-conditioned concrete box set on 44 air bearings, with its 0.3 m thick walls (R) lined with a copper plate (S) to shield from electromagnetic interference and covered by fibreglass wedges (T). The wedges are 1 m long, giving the chamber an ambient sound level of 35 dB above 100 Hz; most of the sound comes from conduction through the jet pipe from the laboratory outside the chamber. The inside dimensions of the chamber from wedgetip to wedgetip are $7.6 \times 5 \times 5$ m. Air feeding the jet originates at an inlet (A) in the air-conditioned room which contains the anechoic chamber; it is piped to a 7-stage blower (B) driven by a 40 h.p. DC motor (C) and located outside the main building, its outlet connected to the nozzle in the anechoic chamber via a 77 m long iron pipe of 15.25 cm diameter. Mufflers and vibration isolation couplings located on either side of the blower minimize the transmitted sound and vibration. Between the blower and nozzle are several flow conditioning devices. An electrostatic filter (D) removes any dust or dirt (95% of 2 μm particles) which might break hot-wire probes. A controlled cooling coil (E) allows the air to be brought back to room conditions for accurate hot-wire measurements. Large-radius elbows (1 m radius) are used at all bends to minimize secondary flow. Seven screens (F) (24 and 40 mesh) and one honeycomb section (G) (0.48 cm cell, 5.08 cm thick) remove any asymmetry and swirl of the flow and are shown by short line segments between the last bend and the nozzle (J).

The DC blower motor is controlled by a Polyspede HP-3 Adjustable Speed Drive System, with adjustments for speed regulation, torque limits and acceleration. At low speeds, the controller 'hunts' for the set point and introduces some low-frequency oscillations of the blower (≈ 0.3 Hz), but this is not significant at jet speeds $U_e \geqslant 5$ m s^{-1} ($St_D < 2$); in this study, the speed range used was $7 < U_e < 21$ m s^{-1}. This frequency is three decades lower than the excitation frequency and at least one decade below the lowest observed modulation frequencies. At all velocities used, the exit-centreline total r.m.s. velocity fluctuations (excluding excitation) were $u'/U_e \leqslant 0.1\%$.

Bulk excitation, where an acoustic source is located upstream of the nozzle to add a longitudinal component of perturbation to the mean flow, was provided through the walls of the diffuser (L) by four speakers (M) angled downstream. Perturbations from

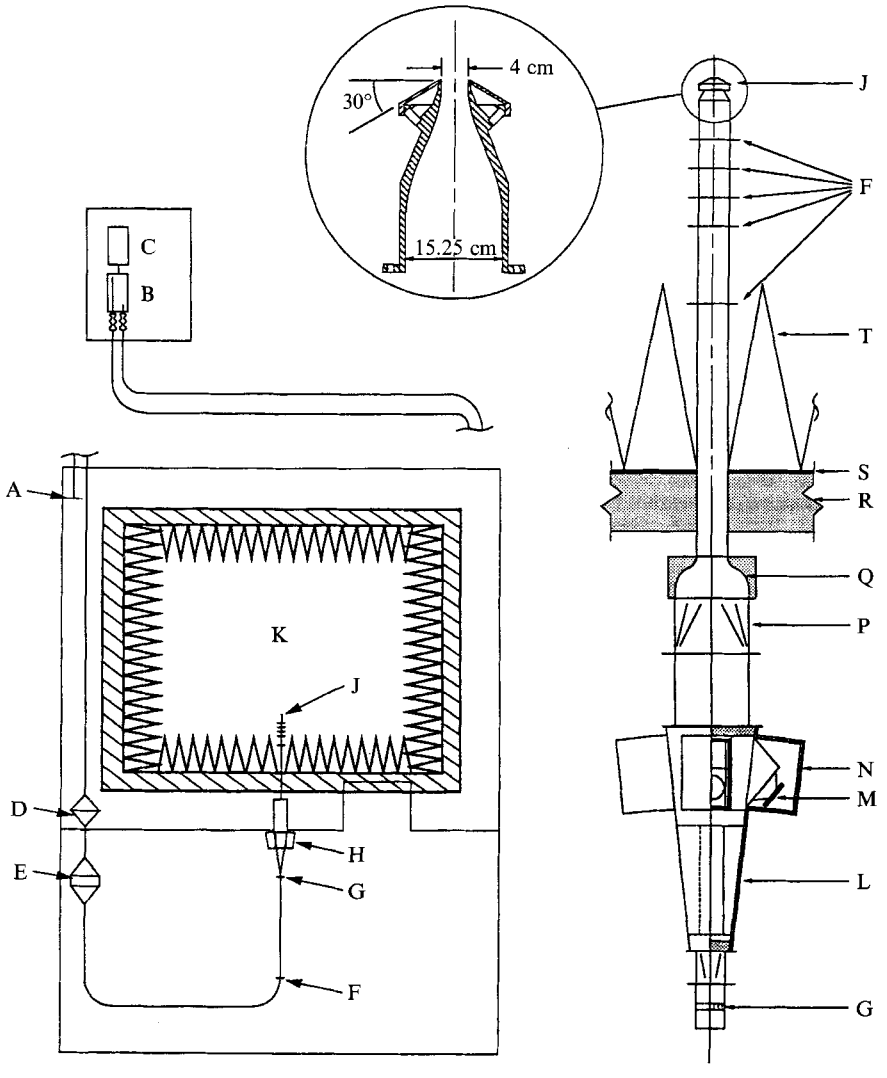

FIGURE 14. Anechoic chamber and jet facility: A, air intake; B, compressor with mufflers and vibration-isolating couplings; C, DC motor; D, electrostatic filter; E, heat exchanger; F, screens; G, honeycomb; H, bulk excitation device; J, nozzle; K, anechoic chamber; L, diffuser; M, speaker; N, speaker housing; P, square-to-round section; Q, contraction; R, chamber wall; S, copper plate for electrical shielding; T, fibreglass wedges.

the speakers pass through a wire mesh and cloth screen which are flush with the walls of the diffuser and provided to prevent disturbance of the flow by the openings of speaker housings (N) into the diffuser. The transfer function of this facility between the speakers and the jet nozzle was reported by Bridges (1990).

Constant-temperature hot-wire anemometers (CTAs), manufactured by AA Labs (Israel), were used to obtain the velocity data. The hot-wire signals were not linearized with an analog circuit but were converted to velocity by computer, having first been calibrated using King's law for each wire ($E^2 = A + B\,U^c$) to determine A, B and c. In order to improve the signal-to-noise ratio, the CTA on-board offset and gain features were employed to cover a domain of $-0.5\,\mathrm{V} \leqslant E \leqslant -8\,\mathrm{V}$ over a range of, say, $0 \leqslant U \leqslant 20\,\mathrm{m\,s^{-1}}$. This did not have a deleterious effect on the coefficient of

determination of the least-squares calibration fit (typically, $R^2 \geqslant 0.99999$). Compensation was provided in software for small changes in temperature, pressure and humidity; when these values changed significantly, the probes were recalibrated. Two types of single-wire probes were employed, one with 5 mm long prongs and one with 25 mm long prongs. Both used 4 μm tungsten–rhodium wire and had an effective length of approximately 2 mm. The overheat ratio used was 1.4.

All data were acquired on a Masscomp MC5500 computer running on real-time UNIX. To eliminate high-frequency transmission noise and aliasing, all hot-wire signals were sent to the computer through coaxial cables and lowpass filtered using eighth-order Krohn-Hite analog filters just before connection to the sample-and-hold board. The hot-wire data were sampled in differential mode with a 12-bit a/d converter through a bank of sample-and-hold amplifiers.

Some of the data analysis was done on a second MC5500 computer. Given the amount of data to be analysed, this processing was eventually off-loaded to a Cray Y-MP at NASA Ames Research Center. The processing speed of the Cray was typically 500 times faster than the MC5500 for dimension calculations.

A two-channel digital Ono Sokki 920 spectrum analyser was used for real-time checks of CTA voltage spectra and to determine the forcing amplitude from the hot-wire probe placed at the jet exit. Using the calibration function, the normalized r.m.s. velocity fluctuation can be expressed in a Taylor expansion up to second order as $u'/U_e = (Q^2 e'^2 + 1.5\, P^2 e'^4)^{\frac{1}{2}}$, where e' and u' are r.m.s. voltage and velocity respectively, E and U are mean voltage and velocity respectively, $Q = [2\, E\, U_e^{-c}/B\, c]$ and $P = [Q/(2\, E)\, \{1 + (1-c)\, Q\, E\}]$. Under common operating conditions, the second-order correction is essentially negligible, and the transformation from voltage to velocity is linear to a good approximation. Therefore, excitation amplitude was computed using $u_f'/U_e = 2\, E\, U_e^{-c}\, e_f'/(B\, c)$ from the calibration and spectrum analyser data.

A.2. *Measurement procedures*

Data for analysis were obtained using hot wires. A long-prong probe was placed in the nozzle exit plane at approximately a 30° angle to the jet axis at $y/R \approx 0.4$ such that the probe body was out of the flow to avoid shear-layer tones (Hussain & Zaman 1978). This reference probe was used to measure u_f' (the exit r.m.s. velocity fluctuations at the forcing frequency) and U_e (jet exit velocity). A measurement probe aligned with the jet axis was placed on the centreline in the jet potential core at axial locations in the range $1.5 \leqslant x/D \leqslant 3.0$; all data presented were taken at $r/D = 0$. Although the flow is spatially developing, there are global modes present due to feedback from the downstream flow events. Therefore, any measurement location is adequate so long as it is sufficiently far downstream to register fluctuations due to pairings but within the potential core so that shear-layer turbulence does not dominate the signal. The excitation frequency used in all cases was 264 Hz (with the exception of data presented in figure 1), since that corresponds to a resonance frequency of the jet settling chamber, permitting high excitation amplitudes. The sampling frequency was chosen typically to be 40 times the dominant frequency (to provide high temporal resolution for ν and λ_1 calculations) and was therefore 2640 Hz for SDP and QCA and 5280 Hz for SP and NPMP.

The phase differences in § 2.4 were calculated from the fundamental and subharmonic phases in the following way. First, the velocity perturbation is defined as follows: $u(t) = a\cos(2\pi f_{ex}\, t + \phi_f) + b\cos(\pi f_{ex}\, t + \phi_s)$, where the first and second terms represent the fundamental and subharmonic respectively. The phase difference is then defined as $\phi = \phi_s - \frac{1}{2}\phi_f$. The input ϕ_{in} was fixed using a phase-locked generator; the phase

shifts between the forcing signal and the jet exit perturbation were computed for both frequency components from the cross-spectrum and used to determine jet exit phases, from which ϕ_{out} was calculated.

A.3. *Data analysis tools*

The state of the system was determined in various ways: time traces and spectra were observed and phase portraits and Poincaré sections were constructed using the time-delay method. In every case, spectra were averaged over several hundred realizations; phase portraits cover 100–500 orbits of the attractor, and Poincaré sections include 1000–10000 (typically 2500) intersections at each plane designated. The time delay was chosen to be the first minimum of the mutual information function (Fraser & Swinney 1986). The minimum required embedding dimension m_{min} was estimated using the false-near-neighbour algorithm of M. B. Kennel, R. Brown & H. D. I. Arbabanel (1992, private communication) and was used to select the embedding dimension to calculate the Lyapunov exponent.

Attractor dimension ν was estimated using the Grassberger–Procaccia (1983) method, in which a correlation integral $C(r)$ is used to measure how the number of points increase with r within a hypersphere of radius r on the reconstructed attractor. The correlation integral is expected to vary as $C(r) \sim r^{\nu}$, where ν is the 'correlation dimension'. Computing the derivative (using cubic splines) of $\log C(r)$ versus $\log r$, ν is taken to be the value of the derivative over a range of r where the derivative is (nearly) constant (i.e. within some deviation limit ϵ, typically 10%). This range is called the 'scaling region' and the ratio of distances corresponding to its endpoints is called the 'scaling factor'. If there is no range where the derivative is constant, it is said that there is a 'lack of scaling'. The range of scales (over which the attractor has dimension ν) proves to be valuable input for the choices of minimum and maximum limits r_{min} and r_{max} for selecting neighbouring trajectories in the Wolf *et al.* (1985) algorithm to estimate the largest Lyapunov exponent λ_1. Correlation dimension calculations were carried out for embedding dimensions $m = 1$–10 and are reported for $m = m_{min}$ (as well as others for NPMP). In all cases, time series of length $\geqslant 10^5$ were used (10^6 in the case of NPMP) comprising at least 2500 orbits of the attractors (since the sample frequency was 40 times the dominant frequency).

The choice of r_{min} and r_{max} has a strong effect on the results of Wolf's algorithm; choosing neighbours whose separation is within the noise range will result in high estimates of λ_1, while choosing widely separated trajectories will yield low values. A number of tests using synthetic and laboratory data confirmed that the scaling range extracted from the correlation integral would yield correct values of λ_1. The λ_1 estimates were confirmed using the Kruel–Eiswirth (1992, private communication) algorithm for the Lyapunov spectrum. In the four main cases, the Kolmogorov entropy was estimated using the Grassberger–Procaccia (1983) method and was found to agree qualitatively with the Wolf method, in that periodic attractors had $\lambda_1 \approx 0$ and chaotic attractors had a positive entropy slightly larger than the estimated λ_1.

The analysis was performed on CTA voltages (measured by the a/d converter) rather than velocity. There are several reasons to do this. One important observation is that the transformation from voltage to velocity fluctuations in CTAs is a diffeomorphism (thus preserving diffeomorphic invariants; see the equations in §A.1). No information about the attractor is lost or altered; this was verified in several test cases for ν, λ_1 and size of scaling range. Therefore, for $U > 0$ using common conditions of a CTA, analysis can be made with E instead of U. This is very important, because it allows other transformations to be made to E that will improve the signal-to-noise

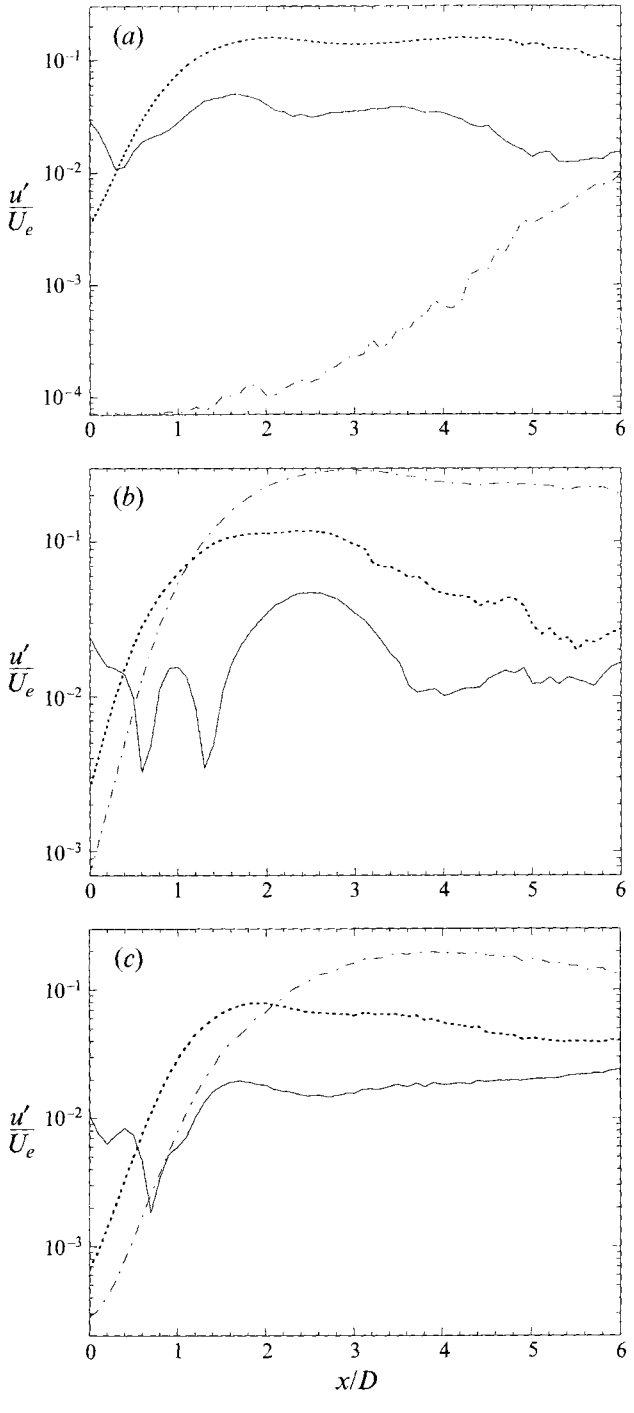

FIGURE 15. Spatial development of spectral components (——, f; - - - -, s; —·—, q) for (a) stable pairing at $St_D = 0.85$, $a_f = 2.9\%$, $Re_D = 3.3 \times 10^4$; (b) stable double pairing at $St_D = 1.19$, $a_f = 2.4\%$, $Re_D = 2.3 \times 10^4$; (c) quarter-harmonic chaotic attractor at $St_D = 1.19$, $a_f = 1.06\%$, $Re_D = 2.3 \times 10^4$.

ratio, specifically to subtract the mean and amplify the signal before transmission to the a/d converter; such a function $E_2 = k_1 + k_2\ E_1$ is also diffeomorphic. Another advantage is that data handling and storage can be done with integer files rather than with larger, slower floating-point files. This is particularly useful when analysing numerous (hundreds!), voluminous data sets, as was the case here. One further advantage is that correlation dimension plots have as their abscissa the logarithm of phase-space distance, which corresponds directly to the number of bits of the a/d converter. Some related details can be found in Broze (1992).

A.4. *Streamwise development of spectral components*

The amplitude evolutions of the fundamental f, subharmonic s and quarter-harmonic q were measured along the jet centreline for $0 \leqslant x/D \leqslant 6$ for SP, SDP and QCA (figure 15). Near the exit, the signal consists of the velocity fluctuations from the imposed plane-wave forcing and the induced velocity from downstream vortices and their interactions. Often, the forcing dominates in this region, reflecting the fact that the probe, on the centreline, is rather far from the shear layer where rollup is occurring. However, since we have sought to capture the *global* dynamics of the jet, the centreline is the best measurement location; correspondingly, we have measured the streamwise growths there as well.

For SP (figure 15*a*), f initially decreases since the forcing amplitude decays faster than the perturbation induced by the rolled-up vortices grows. At $x/D = 0.3$, f begins to increase; its growth rate decreases near $x/D \approx 0.8$ but shortly increases again, peaking at $x/D \approx 1.6$. The slight bump at $x/D \approx 0.8$ is the rollup location, but before any decay can occur f is augmented as the first harmonic of s, which has become nonlinear and has begun to saturate. The subharmonic grows exponentially from its feedback-induced amplitude of approximately 0.3% and saturates near $x/D = 1.8$–2.2. These rollup and pairing locations correspond to those found for SP by Bridges & Hussain (1992) using vorticity-based coherent structure eduction. The growth of q is quite weak, reaching approximately 10% of s by $x/D = 6$.

For SDP (figure 15*b*), f again initially decays from its high initial value, reaching a brief plateau near $x/D \approx 0.4$ before decaying. It rises again at $x/D \approx 1$ as a harmonic of s, decays, and rises at $x/D \approx 3$ again as a harmonic of q. The growth of s is the result of the fact that there are two pairing locations for SDP, one for the leapfrog motion of the leading pair (at $x/D \approx 1$ from Bridges & Hussain) and the other for the trailing pair ($x/D \approx 1.7$); this is quickly followed by the saturation of q, producing a harmonic at s. The combined effect is thus a wide saturation plateau for s. The quarter-harmonic grows monotonically and saturates at $x/D \approx 3$.

The evolution of f for QCA (figure 15*c*) again shows initial decay, but shows a clear peak at $x/D \approx 0.4$. It decays, then rises as a harmonic of s, finally peaking at $x/D \cong 1.7$. After that, it rises only gradually as q develops rather slowly. The subharmonic grows exponentially and saturates near $x/D \approx 1.8$. The q amplitude grows slowly and does not peak until $x/D \approx 4$, reflecting the fact that second pairings are not stabilized at a fixed location, but shift up and down the axis and often do not occur at all.

REFERENCES

ARONSON, I. S., GAPONOV-GREKHOV, A. V. & RABINOVICH, M. I. 1988 *Physica* **33D**, 1.

AUBRY, N. HOLMES, P., LUMLEY, J. L. & STONE, E. 1988 *J. Fluid Mech.* **192**, 115.

BERGÉ, P., DUBOIS, M., MANNEVILLE, P. & POMEAU, Y. 1980 *J. Phys. (Paris) Lett.* **41**, L344.

BERGER, W. D. 1993 Visualization study of some vortex interactions in a circular jet. Senior Honors thesis, University of Houston.

BIRINGEN, S. & PELTIER, L. J. 1990 *Phys. Fluids* A **2**, 754.

BONETTI, M. & BOON, J.-P. 1989 *Phys. Rev* A **40**, 3322.

BRANDSTÄTER, A. & SWINNEY, H. L. 1987 *Phys. Rev.* A **35**, 2207.

BRIDGES, J. E. 1990 Application of coherent structure vortex sound theories to jet noise. PhD dissertation, University of Houston.

BRIDGES, J. E. & HUSSAIN, F. 1992 *J. Fluid Mech.* **240**, 469.

BROWN, G. L. & ROSHKO, A. 1974 *J. Fluid Mech.* **64**, 775.

BROZE, G. 1992 Chaos in an 'open' flow: experiments in transitional jets. PhD dissertation, University of Houston.

BROZE, G. & HUSSAIN, F. 1991 In *Nonlinear Dynamics of Structures* (ed. R. Sagdeev, U. Frisch, F. Hussain, S. Moiseev & N. Erokhin), pp. 391–417. World Scientific.

BUELL, J. C. & HUERRE, P. 1988 In *Proc. Summer Institute of the Center for Turbulence Research*, NASA Ames–Stanford University, pp. 19–27.

CHOMAZ, J. M., HUERRE, P. & REDEKOPP, L. G. 1988 *Phys. Rev. Lett.* **60**, 25.

CORCOS, G. M. & SHERMAN, F. S. 1984 *J. Fluid Mech.* **139**, 29.

CROW, S. C. & CHAMPAGNE, F. H. 1971 *J. Fluid Mech.* **48**, 567.

DEISSLER, R. J. 1985 *J. Statist. Phys.* **40**, 371.

DEISSLER, R. J. 1989 *J. Statist. Phys.* **54**, 1459.

DEISSLER, R. J. & KANEKO, K. 1987 *Phys. Lett.* A **119**, 397.

DIMOTAKIS, P. E. & BROWN, G. L. 1976 *J. Fluid Mech.* **78**, 535.

FIEDLER, H. E. 1988 *Prog. Aerospace Sci.* **25**, 231.

FRASER, A. & SWINNEY, H. L. 1986 *Phys. Rev.* A **33**, 1134.

FREYMUTH, P. 1966 *J. Fluid Mech.* **25**, 683.

GLAUSER, M., ZHENG, X. & DOERING, C. R. 1991 *Bull. Am. Phys. Soc.* **36**, 2621.

GRASSBERGER, P. & PROCACCIA, I. 1983 *Physica* **9D**, 189.

GRINSTEIN, F. F., ORAN, E. S. & BORIS, J. P. 1990 *Phys. Rev. Lett.* **64**, 870.

GUCKENHEIMER, J. 1986 *A. Rev. Fluid Mech.* **18**, 15.

HUERRE, P. & MONKEWITZ, P. A. 1985 *J. Fluid Mech.* **159**, 151.

HUERRE, P. & MONKEWITZ, P. A. 1990 *A. Rev. Fluid Mech.* **22**, 472.

HUSAIN, H. S. & HUSSAIN, A. K. M. F. 1986 *Bull. Am. Phys. Soc.* **31**, 1696.

HUSAIN, H. S. & HUSSAIN, A. K. M. F. 1989 In *Advances in Turbulence 2* (ed. H. Fernholz & H. Fiedler), pp. 96–101. Springer.

HUSSAIN, A. K. M. F. 1986 *J. Fluid Mech.* **173**, 303.

HUSSAIN, A. K. M. F., HUSAIN, H. S., ZAMAN, K. B. M. Q., TSO, J., HAYAKAWA, M., TAKAKI, R. & HASAN, M. A. Z. 1986 *AIAA Paper* 86-0235.

HUSSAIN, A. K. M. F. & ZAMAN, K. M. B. Q. 1978 *J. Fluid Mech.* **87**, 349.

HUSSAIN, A, K. M. F. & ZAMAN, K. M. B. Q. 1980 *J. Fluid Mech.* **101**, 493.

HUSSAIN, A. K. M. F. & ZAMAN, K. M. B. Q. 1981 *J. Fluid Mech.* **110**, 39.

JENKINSON, J. P. & HUSSAIN, A. K. M. F. 1987 *Bull. Am. Phys. Soc.* **32**, 2026.

KEEFE, L., MOIN, P. & KIM, J. 1992 *J. Fluid Mech.* **242**, 1.

KEEFE, L. R. 1987 *Bull. Am. Phys. Soc.* **32**, 2070.

KELLY, R. E. 1967 *J. Fluid Mech.* **27**, 657.

KIBENS, V. 1980 *AIAA J.* **18**, 434.

KLINE, S. J., REYNOLDS, W. D., SCHRAUB, F. A. & RUNSTADLER, P. W. 1967 *J. Fluid Mech.* **30**, 741.

LANFORD, O. E. 1982 *A. Rev. Fluid Mech.* **14**, 347.

LAUFER, J. & MONKEWITZ, P. 1980 *AIAA Paper* 80–0962.

LIBCHABER, A. & MAURER, J. 1980 *J. Phys. (Paris) Lett.* **41**, C3–51.

LUMLEY, J. L. 1981 In *Transition and Turbulence* (ed. R. E. Meyer), p. 215. Academic.

MANKBADI, R. R. 1985 *J. Fluid Mech.* **160**, 385.

MICHALKE, A. 1965 *J. Fluid Mech.* **23**, 521.

MICHALKE, A. 1971 *Z. Flugwiss.* **19**, 159.

MITSCHKE, F., MÖLLER, M. & LANGE, W. 1988 *Phys. Rev.* A **37**, 4518.

MONKEWITZ, P. A. 1988 *J. Fluid Mech.* **188**, 223.

MORKOVIN, M. V. 1988 *AIAA Paper* 88-3675.

PATNAIK, P. C., SHERMAN, F. S. & CORCOS, G. M. 1976 *J. Fluid Mech.* **73**, 216.

PIERREHUMBERT, R. T. & WIDNALL, S. E. 1981 *J. Fluid Mech.* **102**, 301.

ROHLING, T., GHIA, K. N., OSSWALD, G. A. & GHIA, U. 1990 *Bull. Am. Phys. Soc.* **35**, 2229.

RUELLE, D. 1990 *Proc. R. Soc. Lond.* A **427**, 241.

RUELLE, D. 1991 In *New Perspectives in Turbulence* (ed. L. Sirovich), pp. 123–138. Springer.

SREENIVASAN, K. R. 1985 In *Fundamentals of Fluid Mechanics* (ed. S. H. Davis & J. L. Lumley), pp. 41–67. Springer.

SREENIVASAN, K. R. 1986 In *Dimensions and Entropies in Chaotic Systems* (ed. G. Mayer-Kress), pp. 222–230. Springer.

THEILER, J. 1986 *Phys. Rev.* A **34**, 2427.

VAN ATTA, C. W. & GHARIB, M. 1987 *J. Fluid Mech.* **174**, 113.

VASTANO, J. & PULLIAM, T. 1989 In *Proc. ASME-ASCE Forum on Chaotic Dynamics, UCSD, La Jolla, CA, July 10–12, 1989.*

VIRK, D. P. S. 1989 Numerical study of feedback and subharmonic resonance in free shear layers. MS thesis, University of Houston.

WILLIAMS-STUBER, K. & GHARIB, M. 1990 *J. Fluid Mech.* **213**, 29.

WOLF, A., SWIFT, J. B., SWINNEY, H. L. & VASTANO, J. 1985 *Physica* **16D**, 285.

YOKUDA, S. & RAMAPRIAN, B. R. 1990 *Phys. Fluids* A **2**, 784.

ZAMAN, K. M. B. Q. & HUSSAIN, A. K. M. F. 1980 *J. Fluid Mech.* **101**, 449.